# Supporting Information

## Cofactor-independent photoenzymatic, reductions with water mediated by rGQDs

Li Qiao, [#a] Xiaoyu Li, [#a] Yongjian Jinag, [a] Zhiguo Wang, *[b] Wei Ye, *[a] Anming Wang, *[a] Peng Gao *[a] and Roger A. Sheldon *[c, d]

[a] Key Laboratory of Organosilicon Chemistry and Materials Technology, Ministry of Education; College of Material, Chemistry and Chemical Engineering, Hangzhou Normal University, Hangzhou, Zhejiang 311121, P. R. China.

[b] School of Basic Medical Sciences, Hangzhou Normal University, Hangzhou, 311121 (China).

[c] Molecular Sciences Institute, School of Chemistry, University of the Witwatersrand, PO Wits. 2050, Johannesburg, South Africa.

[d] Department of Biotechnology, Section BOC, Delft University of Technology, Van der Maasweg 9, 2629 HZ Delft, the Netherlands.

[#] They contributed equally to this work.

**Corresponding author. Zhiguo Wang; zhgwang@hznu.edu.cn; Wei Ye; yewei@hznu.edu.cn; Anming Wang; waming@hznu.edu; Peng Gao; gaopeng@hrbeu.edu.cn; Roger A. Sheldon; roger.sheldon@wits.ac.za, r.a.sheldon@tudelft.nl.*

## 1. Experimental section

### 1.1 Materials

Unless otherwise stated, all materials were commercially available. All solvents were of analytical grade and used without further purification. The *Escherichia coli Escherichia coli* (*E. coli* DH5α and *E. coli* BL21(DE3)) used in the study were obtained from Stratagene and Novagen. The used endonucleases and primers in the study were synthesized or purchased from Shanghai Generay Biotech (Shanghai) Co., Ltd. Antibiotics (chloramphenicol, kanamycin, and ampicillin) were purchased from Sangon Biotech (Shanghai) Co., Ltd. The non-standard amino acid *p*-Azide-L-phenylalanine (*p*AzF) was obtained from Artis Biotech Co., Ltd. The inducers (anhydrotetracycline hydrochloride (aTc), L-(+)-arabinose) were obtained from Sigma-Aldrich Co., Ltd. $NADP^+$ was obtained commercially from J&K Scientific Co., Ltd. 3,5-bis(trifluoromethyl)acetophenone (3,5-BTAP), 3-chloro-1-phenyl-1-propanone, 1-methyl-1,2,3,4-tetrahydroisoquinoline, 1-methyl-3,4-dihydroisoquinolin, 3-phenylpropanol, cinnamaldehyde, 3-chloro-1-phenyl-1-propanol and 3-chloro-1-phenylpropan-1-one were purchased from Shanghai Energy Chemical Co., Ltd. All other biological reagents were purchased from Sangon Biotech (Shanghai) Co., Ltd. while all other chemical reagents were purchased from Sinopharm Chemical Reagent (Shanghai) Co., Ltd. and were used without further treatment.

### 1.2 DNA Sequences Information

***AKR***

ATGCTGTACAAAGAACTGGGCCGTACCGGTGAAGAAATTCCGGCCTTAGGC
TTAGGCACCTGGGGTATTGGCGGCTTTGAAACCCCGGATTATTCTCGCGATG
AAGAAATGGTGGAACTGTTAAAAACCGCAATTAAAATGGGCTATACCCATA
TTGATACCGCAGAATATTATGGCGGCGGTCATACCGAAGAACTGATTGGTAA
AGCCATTAAAGATTTTCGTCGCGAGGATCTGTTTATTGTGTCTAAAGTGTGG
CCGACCCATCTGCGCCGTGATGATCTGCTGCGCTCTCTGGAAAATACCCTG

AAACGTTTAGATACCGATTATGTGGATCTGTATCTGATTCATTGGCCGAATCC
GGAAATTCCGCTGGAAGAAACCCTGAGTGCAATGGCAGAAGGCGTGCGTC
AGGGCTTAATTCGCTATATTGGTGTGAGTAATTTTGATCGTCGCCTGCTGGA
AGAAGCCATTTCTAAATCACAGGAACCGATTGTTTGTGATCAGGTTAAATAT
AATATTGAAGATCGCGATCCGGAACGCGATGGTTTACTGGAATTTTGTCAG
AAAAATGGCGTGACCTTAGTTGCCTATAGTCCGTTACGTCGTACCTTACTGA
GTGAAAAAACCAAACGCACCTTAGAAGAAATTGCCAAAAATCATGGTGCC
ACCATATACCAGATTATGTTAGCATGGCTGTTAGCCAAACCGAATGTGGTTG
CAATTCCGAAAGCAGGTCGTGTTGAACATCTGCGCGAAAATCTGAAAGCA
ACCGAAATTAAACTGAGCGAAGAAGAGATGAAACTGCTGGATAGTCTGGG
T

***AoIRED***

ATGACCGACCAGAACCTGCCGGTTACCGTGGCGGGTCTGGGCCCGATGGG
CTCCGCTCTGGCGGCTGCACTGCTGGACCGTGGTCACGACGTTACTGTTTG
GAACCGCTCTCCGGGCAAAGCAGCACCGCTGGTGGCTAAAGGTGCGCGTC
AGGCGGACGACATCGTTGACGCGGTTAGCGCGTCCCGCCTGCTGGTTGTGT
GCCTGGCGGACTACGATGCGCTGTATAGCGCACTGGGTCCGGCTCGTGAAG
CGCTGCGTGGTCGTGTTGTTGTTAACCTGAACTCTGGCACCCCGAAAGAAG
CGAACGAAGCTCTGCGTTGGGCGGAGCGTCACGGTACTGGTTACCTGGAC
GGTGCGATCATGGTTCCGCCGGCAATGGTTGGTCACCCAGGCTCTGTTTTC
CTGTACTCTGGCTCTGCTGAAGTTTTCGAAGAATACAAAGAAACCCTGGCT
GGCCTGGGCGACCCGGTTCACCTGGGTACTGAAGCGGGCCTGGCAGTTCT
GTACAACACCGCGCTGCTGTCTATGATGTACAGCTCTATGAACGGTTTTCTG
CATGCTGCGGCACTGGTGGGTTCTGCAGGTGTTCCGGCTGCGGAGTTCACC
AAACTGGCTGTTGACTGGTTTCTGCCGGCTGTGATCGGTCAGATCATCAAA
GCGGAAGCGCCGACCATCGACGAAGGCGTTTATCCGGGCGATGCGGGTTC
TCTGGAAATGAACGTGACTACTCTGAAACACATCATCGGCACCTCTCAGGA
ACAGGGTGTTGATACCGAAATCCCGGTGCGTAACAAAGAGCTGCTGGATC
GTGCAGTTGCAGCGGGTTTCGGCGAATCTTCTTACTATTCTGTTATCGAACT

GTGGCGTTAA

***OYE1***

ATGAGCTTTGTTAAAGATTTTAAACCGCAGGCCTTAGGTGATACCAATCTGT
TTAAACCGATTAAAATTGGCAATAATGAACTGTTACATCGTGCCGTTATTCC
GCCGTTAACCAGGATGCGCGCCCTGCATCCGGGTAATATTCCGAATCGCGAT
TGGGCAGTGGAATATTATACCCAGCGTGCACAGCGTCCGGGCACCATGATT
ATTACCGAAGGTGCCTTTATTTCACCGCAGGCCGGCGGCTATGATAATGCCC
CAGGCGTTTGGAGCGAAGAACAGATGGTTGAATGGACCAAAATTTTTAATG
CCATTCATGAAAAAAAATCATTTGTGTGGGTTCAGCTGTGGGTGCTGGGCT
GGGCAGCCTTTCCGGATAATTTAGCACGCGATGGCCTGCGCTATGATAGCGC
CTCAGATAATGTGTTTATGGATGCAGAACAGGAAGCCAAAGCCAAAAAAG
CCAATAATCCGCAGCATAGTCTGACCAAAGATGAAATTAAACAGTATATTAA
AGAATATGTTCAGGCCGCCAAAAATTCTATTGCAGCCGGCGCCGATGGCGT
GGAAATTCATAGCGCAAATGGCTATCTGCTGAATCAGTTTCTCGACCCGCAT
AGTAATACCCGTACCGATGAATATGGCGGTAGTATTGAAAATCGTGCACGCT
TTACCTTAGAAGTTGTGGATGCATTAGTGGAAGCCATTGGTCATGAAAAAG
TGGGCTTACGTCTGTCTCCGTATGGTGTGTTTAATTCAATGTCAGGCGGTGC
AGAAACCGGCATTGTTGCCCAGTATGCCTATGTTGCCGGCGAACTGGAAAA
ACGCGCCAAAGCAGGTAAACGTCTGGCCTTTGTTCATCTGGTTGAACCGCG
TGTGACCAATCCGTTTCTGACCGAAGGCGAAGGTGAATATGAAGGCGGTA
GCAATGATTTTGTGTATAGCATTTGGAAAGGCCCGGTGATTCGTGCAGGCA
ATTTTGCCTTACATCCGGAAGTGGTTCGCGAAGAAGTTAAAGATAAACGTA
CCCTGATTGGCTATGGTCGCTTTTTTATTTCTAATCCGGATCTGGTTGATCGC
TTAGAAAAAGGTCTGCCGCTGAATAAATATGATCGCGATACCTTTTATCAGA
TGTCAGCACATGGCTATATTGATTATCCGACCTATGAAGAAGCACTGAAACT
GGGTTGGGATAAAAAA

***NaCBR***

ACCATCGCACTGAATAATGTTGTTGCCGTGGTGACCGGTGCCGCAGGTGGT

ATCGGTAGAGAACTGGTTAAAGCCATGAAAGCAGCCAATGCAATTGTTATT
GCAACCGATATGGCCCCGAGCGCCGATGTTGAAGGCGCAGACCATTATCTG
CAGCATGATGTTACCAGTGAAGCCGGCTGGAAAGCCGTTGCCGCATTAGCT
CAGGAAAAATATGGTCGTGTTGATGCACTGGTGCATAATGCCGGTATTAGTA
TTGTGACCAAATTCGAAGACACCCCGCTGAGTGATTTTCATCGCGTTAATAC
CGTTAACGTGGATAGTATTATCATCGGTACACAGGTGCTGCTGCCGCTGCTG
AAAGAAGGCGGTAAAGCACGTGCAGGCGGTGCTTCAGTGGTGAATTTTAG
TAGTGTTGGCGGCCTGCGCGGTGCCGCATTCAACGCAGCATATTGTACCAG
TAAAGCAGCAGTTAAAATGCTGAGCAAATGTCTGGGCGCAGAATTTGCCGC
ACTGGGCTATAATATTCGTGTTAATAGTGTGCACCCGGGCGGTATTGATACC
CCGATGCTGGGTAGCATTATGGATAAATATGTGGAACTGGGTGCAGCCCCG
AGCCGTGAGGTGGCACAGGCAGCAATGGAAATGCGTCATCCGATTGGTCG
CATGGGTCGCCCTGCTGAAATGGGTGGTGGCGTTGTTTATCTGTGCAGCGA
TGCAGCCAGCTTTGTGACCTGCACCGAATTTGTTATGGATGGCGGTTTTAGT
CAGGTT

### 1.3 Plasmid Construction, Protein Expression, and Characterization

The plasmid pZE21-GFPaav obtained from Addgene was selected as the target vector to construct a bacterial expression vector of aldo-keto reductase (AKR, PDB ID: 5dan.1; resolution, 2.0 Å) derived from *Thermotoga maritima* MSB8 in GRO MG1655, and it encoded the C-terminus His×6 tag. The target gene was PCR-amplified to obtain AKR with restriction sites. We double-digested pZE21-GFP using restriction enzymes KpnI and Hind III and ligated the AKR gene into pZE21 to acquire pZE21-AKR. The primers designed for the construction of pZE21-AKR are listed in **Table S1**.

Site-directed mutagenesis PCR was performed using pZE21-AKR as a template, and an amber codon (UAG) was introduced at position 114(Y) to replace the tyrosine codon. We selected two mutation sites (114Y-189Q) far from the active site of AKR and named them AKR two-point mutants. Site-directed mutagenesis primers are shown in **Table S2**. The plasmid pEVOL-*p*AzF (tRNA synthetase/tRNA pair) used for the

insertion of *p*AzF (*p*-azido-L-phenylalanine) in *vivo* into proteins which responded to the amber codon, TAG, was from Peter G. Schultz's group at the Scripps Institute.[1] The multipoint mutant gene pZE21-AKR and pEVOL-*p*AzF were co-transformed into MG1655 to prepare an aldehyde ketone reductase expression system.

AKR mutant cells were inoculated into LB medium containing appropriate antibiotics (50 μg·mL$^{-1}$ ampicillin, 34 μg·mL$^{-1}$ chloramphenicol, and 100 μg·mL$^{-1}$ kanamycin), and cultured at 34°C with shaking. When the $OD_{600}$ was 0.6-0.8, we added inducers (0.2% L-(+)-arabinose, 30 ng·mL$^{-1}$ aTc, 1 mM *p*AzF) a final concentration of 1 mmol·L$^{-1}$, after which protein expression was induced for 16 h at 23°C. Cells were treated with ultrasonic disruption and eluted using a 0−300 mM imidazole gradient in PBS buffer (100 mM, pH 7.0) containing 300 mM NaCl. The purified free AKR mutant was concentrated in microsep and washed twice with PBS buffer (100 mM, pH 7.0) to remove NaCl and imidazole. We use sodium dodecyl sulfate polyacrylamide gel electrophoresis (SDS-PAGE) to verify the protein expression and matrix-assisted laser desorption/ionization time-of-flight mass spectrometry (MALDI-TOF MS) to examine the actual relative molecular mass of the obtained protein. Cell debris was removed by centrifugation, after which the resulting supernatant was loaded onto a 5 mL His-Trap HP column (GE healthcare).

The nucleotide sequence of imine reductase AoIRED from *Amycolatopsis orientalis*, ene reductase OYE1 and carbonyl reductase NaCBRwere optimized for *E. coli* codon usage, based on its amino acid sequence. The two gene fragments were synthesized and cloned into digested pET26b to obtain the recombinant plasmids respectively, which were then transformed into *E. coli* BL21 (DE3). Subsequent expression, purification and primary characterization processes are the same with AKR mutant.

**Table S1 Primers required for construction of pZE21-AKR**

| Primer | Sequence (5’→3’) | Restriction-enzyme cutting sites | Tm (℃) |
|---|---|---|---|
| **AKR-pZE21-F** | CGG**GGTACC***ATGCTGTACAAAGAACTGGGCCGTA* | KpnI | 60 |
| **AKR-pZE21-R** | CCC**AAGCTT**TTAGTGGTGGTGGTGGTGGTG *ACCCAGACTATCC* | HindIII | 68 |

Italic, conserved base; Bold, restriction site; Underlined, his-tag label

**Table S2 Primers for AKR sites mutations**

| Primer | Sequence (5’→3’) | Tm (℃) |
|---|---|---|
| **AKR-114Y-F** | GATTATGTGGATCTGTAGCTGATTCATTGGCCG | 62 |
| **AKR-114Y-R** | CGGCCAATGAATCAGCTACAGATCCACATAATC | 62 |
| **AKR-189Q-F** | TTACTGGAATTTTGTTAGAAAAATGGCGTGACC | 62 |
| **AKR-189Q-R** | GGTCACGCCATTTTTCTAACAAAATTCCAGTAA | 62 |

### 1.4 Covalent Cross-Linking of AKR Mutant

Typically, the crosslinker dibenzocycloocta-4a,6a-diene-5,11-diyne (DBA) was dissolved in isopropanol (0.66 mg·mL$^{-1}$), and the solution was added to 1 mL PBS (0.1 mM, pH=7.0) containing the two-point mutant cell lysate. The mixture was irradiated for a certain period in a microwave reactor (Discover CoolMate, CEM, NC, USA) with a cooling module. The molar ratio of azide and alkyne group in the reaction was 1:0.8. The reaction was carried out under 10 W microwave power for 3 min at 10°C. The resulting AKR-CLEs were separated via centrifugation and washed with 1 M NaCl solution.

### 1.5 Enzyme activity

Enzyme activities of wild AKR, AKR-114Y-189Q and AKR CLEs were measured according to the procedures detailed in previously published work from our lab. To a 1 mL system, 100 μL of dihydro-4, 4-dimethyl-2, 3-furandione (dissolved in isopropanol, 6 mg/mL) was added as the test substrate to obtain a final concentration of 3.881 mM. Another 100 μL of NADPH solution (2.5 mg/mL) and a unit amount of enzyme were added and supplemented with PBS (0.02 M, pH 7) to 1 mL. The change in absorbance value at 340 nm was monitored by a UV spectrophotometer (BECKMAN COULTER Du-730) for 1 min. The results are represented in **Table S3** below. The crosslinking of the AKR mutant has hardly affected its activity.

**Table S3 The activity of wild AKR, AKR-114Y-189Q and AKR assembly**

| Entry | Primer | Activity (U/mg) |
|---|---|---|
| **1** | Wild AKR | 1.060±0.020 |
| **2** | AKR-114Y-189Q | 0.932±0.021 |
| **3** | AKR CLEs | 1.041±0.028 |

### 1.6 Preparation of rGQDs

Typically, glucose was dispersed in 40 mL of pure water with magnetic stirring. Then the solution was transferred to a Teflon-lined autoclave (50 mL) and heated at 190°C for 3 h. After the reaction was completed, it was naturally cooled to room temperature. The brown solution was centrifuged to remove the precipitate and retain the supernatant before adding 50 mg of $NaBH_4$. The reaction was stirred at room temperature for 4 h to obtain rGQDs.

### 1.7 Preparation of assembled photoenzyme catalyst rGQDs/AKR

The photoenzyme composite rGQDs/AKR was obtained by electrostatic self-assembly under mechanical oscillation. Typically, aldo-keto reductase aggregates were dispersed in a 5 mL rGQD (5 $mg \cdot mL^{-1}$) suspension with a final concentration of 16 $mg \cdot L^{-1}$. The mixture was shaken continuously at 10°C for 4 hours to obtain hybrid material. Photoenzyme catalysts (rGQDs/AKR) were collected by freeze-drying after centrifugation.

### 1.8 Typical procedures for photoenzymatic catalysis

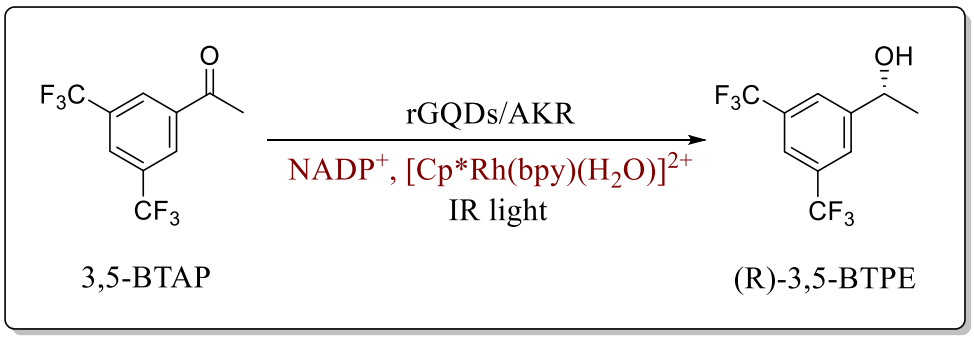


**Scheme S1.** IR-driven photoenzymatic synthesis of (R)-3,5-BTPE

The photoenzymatic synthesis of (R)-3,5-BTPE was carried out in a 45 mL custom-made quartz reactor (**Figure S14**) at 20°C. Typically, 10 mg of photoenzyme catalyst (rGQDs/AKR) was dispersed in 5 mL of PBS buffer (pH=7.0, 100 mM). Then 25 mM of 3,5-BTAP, and 7.8 mM of isopropanol as cosolvent were added to the reaction system.

After that, the reactor was irradiated at AM1.5G with an optical filter (CEL-HXF300, 50 $mW \cdot cm^{-2}$) for 18 hours.

The photoenzymatic synthesis of (R)-3,5-BTPE in the presence of $NADP^+$ and (or) electron mediator was performed in a custom-made quartz reactor at 20°C. 10 mg of photoenzyme catalyst (rGQDs/AKR) was first dispersed in 5 mL of PBS buffer (pH=7.0, 100 mM). Then 25 mM of 3,5-BTAP, 7.8 mM of isopropanol, 0.1 mM of $NADP^+$, and (or) 0.25 mM of $[Cp^*Rh(bpy)(H_2O)]^{2+}$ were added to the reaction system in sequence. The mixture was irradiated at AM1.5G with an optical filter (CEL-HXF300, 50 $mW \cdot cm^{-2}$) for 18 hours.

After the reaction, the target product (R)-3,5-BTPE was extracted from the supernatant in the reaction solution by anhydrous n-hexane. The image of the catalytic product (R)-3,5-BTPE is shown in **Figure S15**. The yield was then determined by chiral high-performance liquid chromatography (HPLC, Agilent 1260 II, CA, USA) with a C18 column (250 mm × 4.6 mm, 5μm particle size, Waters SunFire, MA, USA). Solvent A was methanol, solvent B was water, and the volume ratio of methanol to water was 75:25 (v/v). The temperature of the autosampler was maintained at 20 °C, the volume of each injection was 10 μL, and the flow rate was set at 0.5 $mL \cdot min^{-1}$. The commercial substrate and product were utilized as standard samples to validate the retention times, and data were collected at 210 nm. Enantiomeric excess (ee) of (R)-3,5-BTPE was measured and analyzed by HPLC equipped with a Chiralcel OD-H column (250 mm × 4.6 mm, 5 μm particle size, Daicel, Osaka, Japan), eluted with hexane/isopropanol [98:2 (v/v)] at a flow rate of 1.0 $mL \cdot min^{-1}$ at 20°C, and detected at 210 nm.

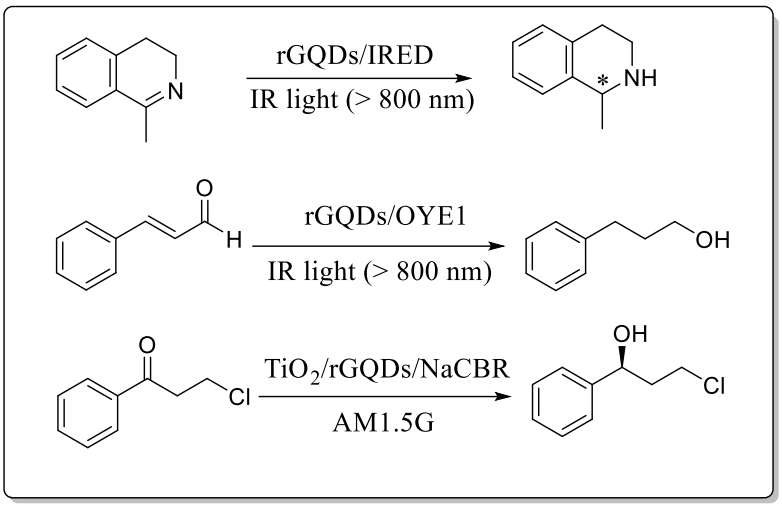


**Scheme S2.** IR-driven photoenzymatic synthesis of 1-methyl-1,2,3,4-tetrahydroisoquinolin (a) and 3-phenylpropanol (b). (c) The photoenzymatic synthesis of (S)-3-chloro-1-phenylpropan-1-ol under simulated sunlight AM1.5G irradiation.

The synthesis of 1-methyl-1,2,3,4-tetrahydroisoquinolin followed the above standard photo-enzymatic reaction conditions except for altering the corresponding photoenzyme to 10 mg AoIRED and 5 mg rGQDs, altering the substrate to 1-methyl-3,4-dihydroisoquinolin, meanwhile using 2% (v/v) DMF as co-solvent. For yield and enantioselectivity detection by HPLC, the mobile phase was changed to n-hexane: isopropanol: diethylamine (96.5:3.5:0.1, v/v), and data were collected at 210 nm. The synthesis and analysis of 3-phenylpropanol followed the standard reaction conditions except for altering the corresponding photoenzyme to 10 mg OYE1 and 5 mg rGQDs, altering the substrate to cinnamaldehyde, and changing solvents A and B to acetonitrile and water (v/v, 65:35), respectively. The data were collected at 265 nm.

To synthesize (S)-3-chloro-1-phenylpropan-1-ol, the bio-inorganic hybrid, $TiO_2$/r-GQDs-NaCBR, was prepared and used to catalyze the enantioselective reduction of 3-chloro-1-phenylpropan-1-one (3-CPP) under simulated sunlight (AM1.5G, 50 $mW \cdot cm^{-2}$) following the above standard reaction conditions. Specifically, the assembly of $TiO_2$ and r-GQDs was first performed by shaking the mixture of 200 mg of $TiO_2$ and 40 mL of rGQDs suspension (5 $mg \cdot mL^{-1}$) at 60℃ overnight. After centrifugal separation and washing with 10 mL of deionized water three times, 10 mg of $TiO_2$/r-GQDs composite was obtained and then assembled with carbonyl reductase (5 $mg \cdot mL^{-}$

[1]) in 5 mL PBS buffer, pH 7.0, at 10°C for 4 h to give $TiO_2$/r-GQDs-NaCBR. The $TiO_2$/r-GQDs-NaCBR can be separated from the reaction mixture by centrifugation and reused several times. After every reaction finished, the yield was determined by HPLC (Agilent 1260 II, CA, USA) with a C18 column (250 mm × 4.6 mm, 5μm particle size, Waters SunFire, MA, USA). Solvent A was n-hexane, solvent B was isopropanol, and the volume ratio of hexane to isopropanol was 90:10 (v/v). The temperature of the autosampler was maintained at 20°C, the volume of each injection was 10 μL, and the flow rate was set at 1 $mL \cdot min^{-1}$. The data were collected at 210 nm. The enantiomeric excess (ee) was analyzed by HPLC equipped with a Chiralcel OD-H column.

**1.9 Isotope-tracer experiment**

1-(2-Chlorophenyl)ethan-1-one was selected as the test substrate for easy to be observed by HRMS. Specifically, 10 mg of AKR and 5 mg of rGQDs were dispersed in 5 mL of PBS buffer (using $D_2O$ as the solvent, pH=7.0, 100 mM). Then 25 mM of 1-(2-Chlorophenyl)ethan-1-one was added to the reaction system. After that, the reactor was irradiated at AM1.5G with an optical filter (CEL-HXF300, 50 $mW \cdot cm^{-2}$) for 18 hours. After the reaction, the reaction mixture was extracted with hexane. The proportion and content of isomers were determined by HPLC, OD-H14325 (**Figure S30**). Solvent A is hexane; solvent B is isopropanol. The volume ratio of hexane to isopropanol was 96:4 (v/v). The column temperature was maintained at 20°C, and the injection volume was 10 μL each time. The detection wavelength was 210 nm, using the corresponding standards to verify the retention times of the substrates and target products. The molecular formula of the product was determined using HRMS (**Figure S31**).

## 2. Characterization

Sodium dodecyl sulfate polyacrylamide gel electrophoresis (SDS-PAGE) was used to characterize gene mutation expression results. Matrix-assisted laser desorption/ionization time-of-flight mass spectrometry (MALDI-TOF MS, Bruker rapifleX) was used to analyze the accurate molecular mass using a Microflex MALDI-TOF mass spectrometer. Confocal laser scanning microscopy (CLSM) images were acquired using a Zeiss LSM 900 confocal laser-scanning microscope. Fluorescent staining was conducted with fluorescein-isothiocyanate (FITC), and then observed with CLSM under 488nm excitation. Transmission electron microscopy (TEM) and high-resolution transmission electron microscopy (HRTEM) were performed on a FEI Talos F200X G2 transmission electron microscope with a field emission gun operated at 200 kV. Field-emission scanning electron microscopy (SEM) images were obtained using a Zeiss Supra 55 scanning electron microscope. Elemental mapping was performed using an energy-dispersive X-ray spectrometer (EDS) attached to the SEM. Raman spectra were taken using a Raman spectrometer (HORIBA LabRAM HR800) with a 532 nm laser excitation. X-ray photoelectron spectroscopy (XPS) measurements were performed by a Thermo Scientific K-Alpha spectrometer system using Al Kα (1486.6 eV) radiation (operated at 12 kV) in the constant analyzer energy mode. The zeta potentials of the samples were measured using a Nanoparticle size and Zeta potential analyzer (Malvern Zetasizer Nano ZS90). Fourier transform infrared (FT-IR) spectra were collected using a Thermo IS-50 FTIR spectrometer with a resolution of 4.0 $cm^{-1}$ in the wavelength range 4000-1100 $cm^{-1}$. X-ray diffraction (XRD) patterns were recorded on a Shimadzu XRD-6000 X-ray diffractometer with Cu Kα radiation at 40 kV and 30 mA. Atomic force microscope (AFM) images were obtained using the Bruker Dimension Icon. Photoluminescence (PL) spectra were measured at an excitation wavelength of 980 nm by using a spectrophotometer (FLS 980) and a Xe lamp (450 W) as excitation sources. UV-Vis-NIR spectra were obtained using a Shimadzu UV-3600 spectrophotometre in the wavelength range 300–1300 nm. The electron spin resonance (EPR) spectra were measured by using a paramagnetic

resonance spectrometer (Bruker EMXplus-6/1) with Xe lamp (300W) as the excitation source.

Electrochemical impedance spectroscopy and photocurrent response test were performed using a three-electrode anaerobic electrochemical quartz chamber connected to a CHI 660E electrochemical station (CH Instruments, TX, USA). The cleaned FTO glass (1 × 1 $cm^2$) coated with 50 μL sample suspension (2 mg of sample is dispersed in a mixture of 700 μL $H_2O$, 200 μL isopropanol and 50 μL of 5wt% Nafion solution), and then dry naturally as the working electrode. A platinum sheet (1 × 1 $cm^2$) and a saturated Ag/AgCl electrode were used as the counter and reference electrodes, respectively. The solution of 0.5 M $Na_2SO_4$ was prepared for the supporting electrolyte.

The photocatalytic water decomposition experiment was conducted in a 500 mL sealed quartz flat bottomed container. Typically, 5mL rGQDs (containing 7.8 mM isopropanol) were added to the reactor. A 300 W xenon lamp (CEL-HXF300, 50 $mW \cdot cm^{-2}$) was used as a visible light source to trigger the photocatalytic reaction. The amount of gas evolution was measured using an on-line gas chromatograph (SP7800, TCD, Ar carrier, Beijing Keruida Limited).

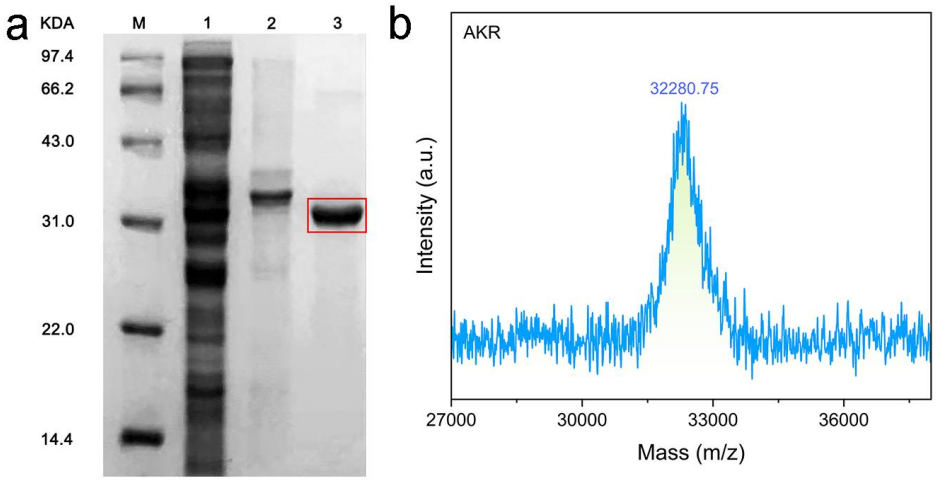


**Figure S1.** (a) SDS-PAGE analysis: lane M, protein marker; lane 1, cell lysate supernatant of AKR mutant; lane 2, cellular insoluble fraction of ADH mutant; lane 3, purified AKR two-point mutant. (b) MALDI-TOF analysis of AKR mutant.

To protect the active site from being overridden or blocked in the cross-linked enzymes, amino acid mutation sites were preferentially used for the covalent immobilization of the protein. As shown in **Figure S1,** the apparent molecular weight of AKR mutant contaning two *p*-azido-L-phenylalanine (*p*AzF) at its 114Y ang 189Q site is about 32 kDa and the red box in SDS-PAGE shows the expression of the two-point mutant (**Figure S1a**). To further verify the correct induction of AKR two-point mutant expression, the enzyme protein was examined by matrix-assisted laser desorption/ionization time-of-flight mass spectrometry (MALDI-TOF MS). As shown in **Figure S1b,** a peak at 32280.75 Da (the molecular weight of the two-point mutation AKR containing *p*AzF was detected as consistent with the theoretical molecular weight (32271.96 Da) appears, which proves that the AKR mutant protein has been successfully expressed and *p*AzF has been inserted into the protein peptide chain at the expected position and the preset position.

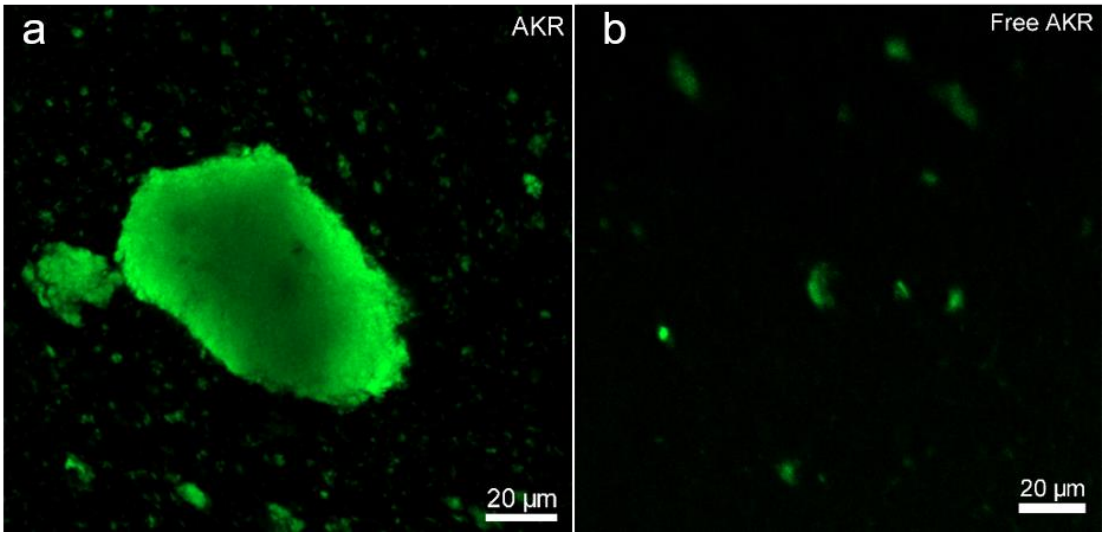


**Figure S2.** (a) CLSM image of AKR-CLEs stained with FITC ($\lambda_{EX}$=488 nm). (b) CLSM image of free AKR stained with Fluorescein Isothiocyanate ($\lambda_{EX}$=488 nm).

The AKR crosslinking aggregates (AKR-CLEs) with plenty of active sites were qualified for binding and converting object substrates in catalytic process. The morphology and microstructure of AKR aggregates were further investigated by a confocal laser scanning microscope (CLSM) image of AKR-CLEs, as shown in **Figure S2a**. The green fluorescence comes from the enzyme protein containing the AKR two-point mutant of *p*AzF. Compared with free enzymes (**Figure S2b)**, AKR-CLEs exhibit coral like morphology with dimensions ranging from 10 to 80 μm. This also agrees with the results verified by transmission electron microscopy (TEM, **Figure S3a**) and scanning electron microscopy (SEM, **Figure S3b**).

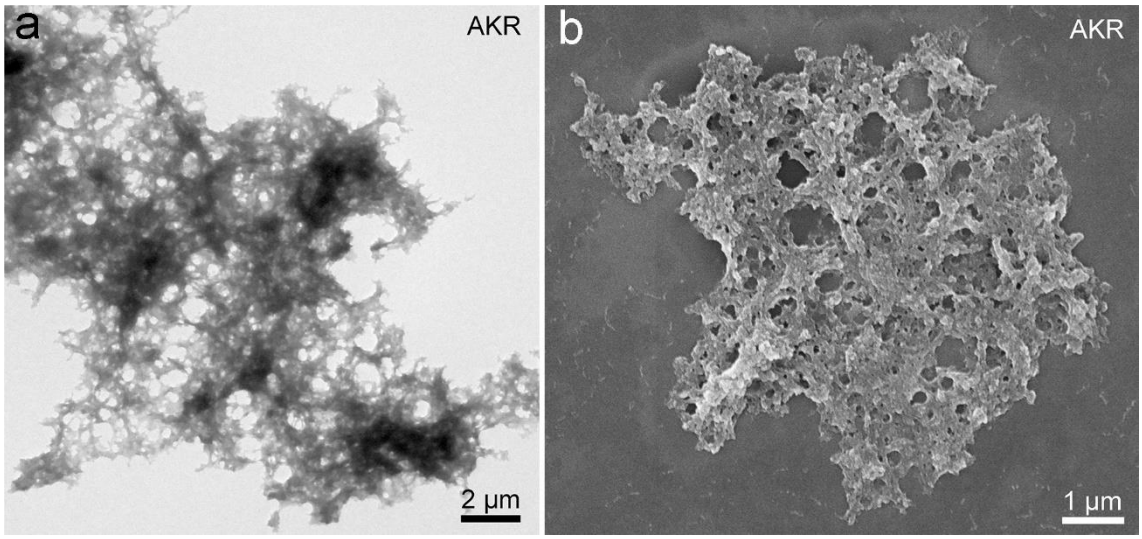


**Figure S3.** (a) TEM image and (b) SEM image of AKR-CLEs.

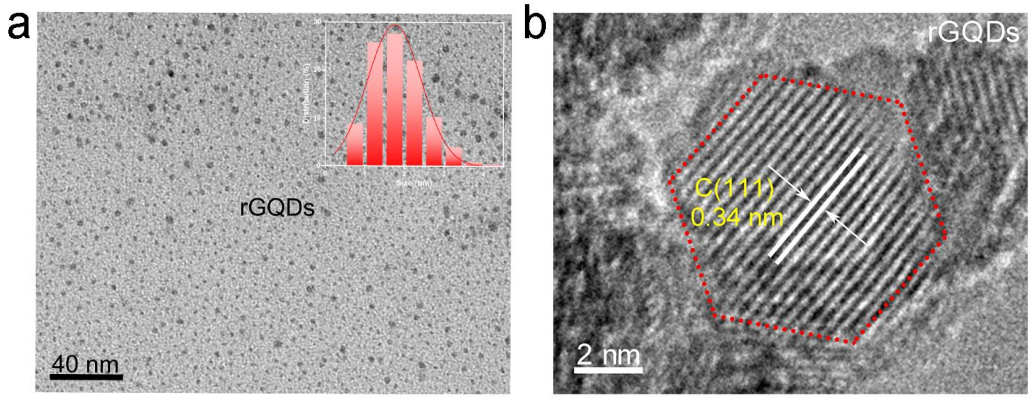


**Figure S4.** (e) TEM image and the size distribution (inset), (f) HRTEM image of rGQDs.

The morphology and size of the rGQDs photocatalyst were first analyzed using TEM examinations. It can be observed that the disk-like rGQDs are normally distributed and their size is about 2 nm (inset of **Figure S4a**). The high-resolution transmission electron microscope (HRTEM) image of rGQDs shows a clear lattice structure with a lattice space of 0.34 nm, which corresponds to the (111) plane of graphite carbon (JCPDS 75-2078) (**Figure S4b**).

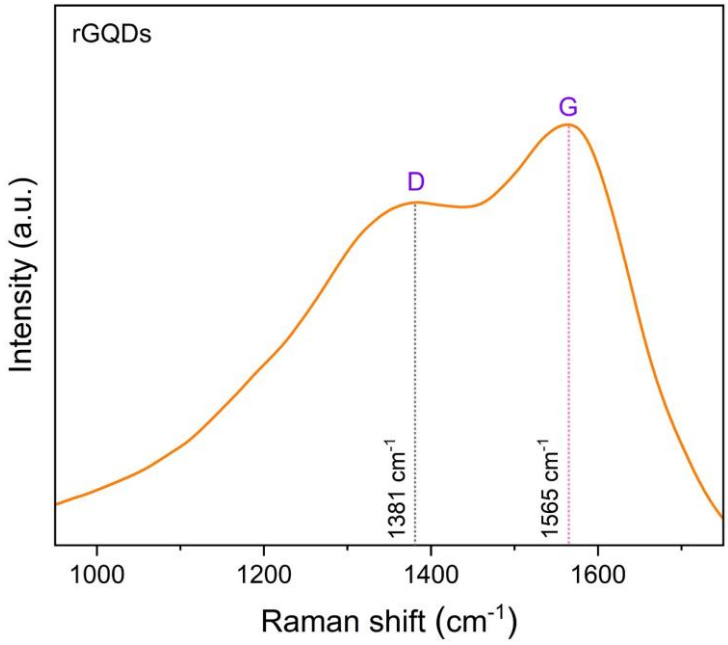


**Figure S5.** Raman spectrum of rGQDs.

The graphene structure in rGQDs was characterized by Raman spectroscopy. As shown in **Figure S5**, two peaks at 1381 and 1565 $cm^{-1}$ attributed to disordered $sp^2$ carbon (D-band) and ordered graphite (G-band), respectively, indicate that the rGQDs consist of 2 or 3 layers.[2]

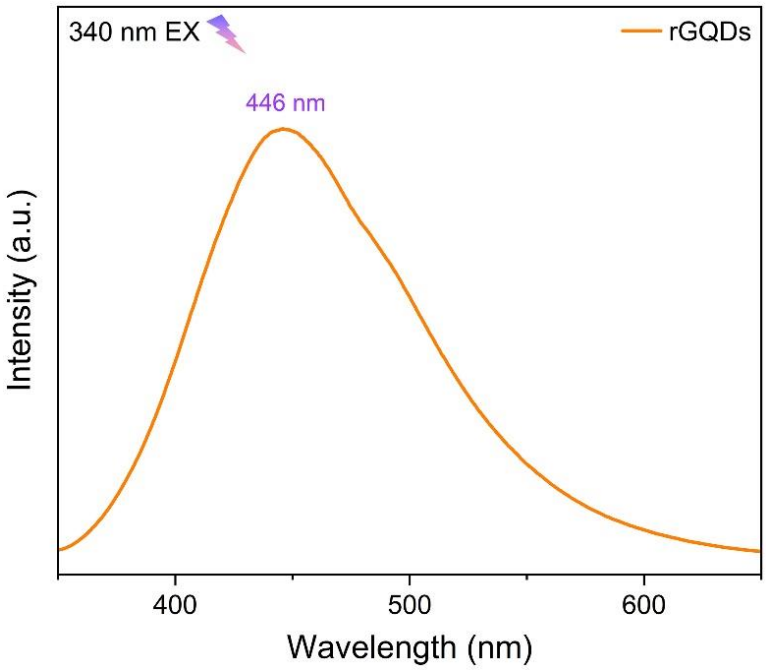


**Figure S6.** PL spectrum of rGQDs with 340 nm excitation.

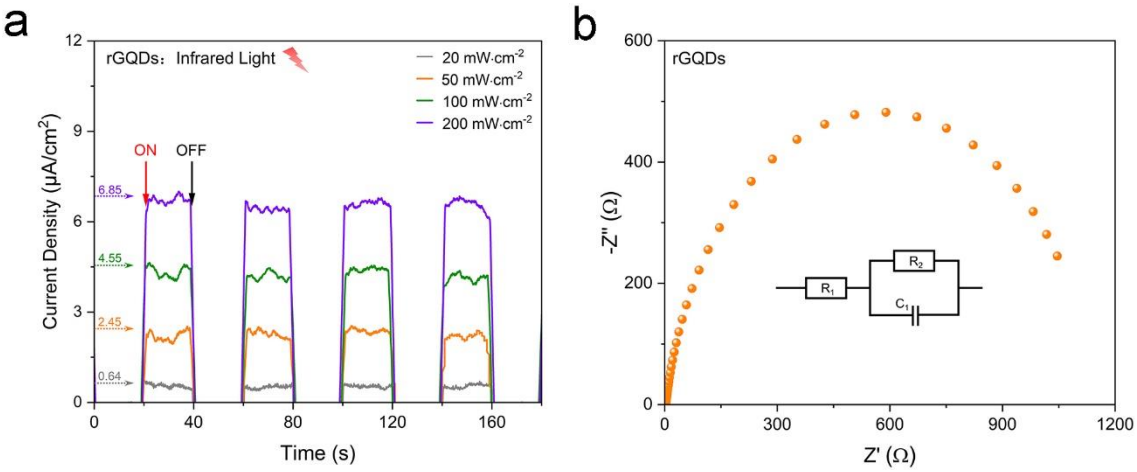


**Figure S7.** (a) Transient photocurrent spectra, (b) electrochemical impedance spectrum of rGQDs measured in $Na_2SO_4$ (0.5 M) solution.

The photoelectric tests proved rGQDs' multiphoton upconversion characteristic (**Figure S7a**). Reasonably, stronger lighting induces higher photocurrent density. In addition, the electrochemical impedance spectroscopy (EIS) also shows a small semicircle in the Nyquist plot of rGQDs, indicating that electron-hole pairs are easier to separate (**Figure S7b**).

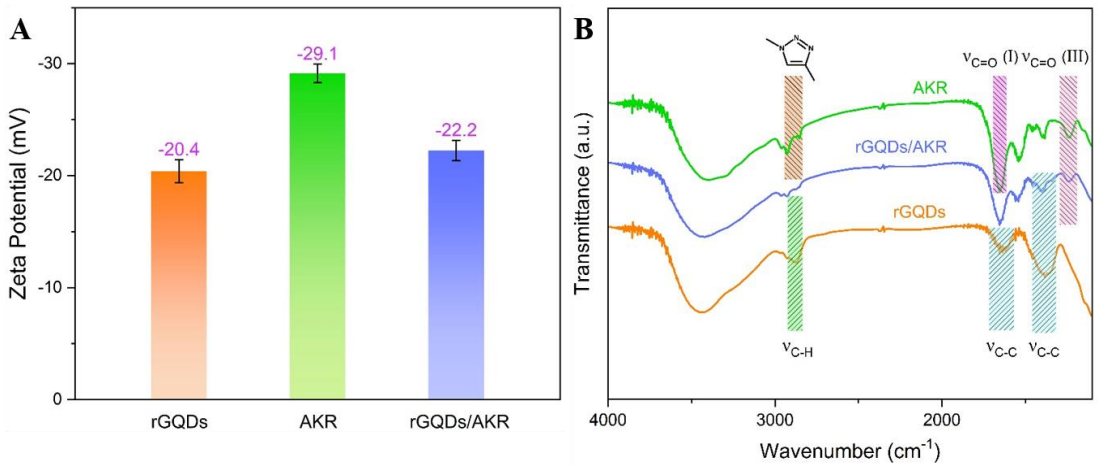


**Figure S8.** Zeta potentials (A) and FT-IR spectra (B) of rGQDs, AKR, rGQDs/AKR.

Fourier transform infrared (FT-IR) analysis was used to study the surface functional groups of the material. Figure S8B shows the FTIR spectra of rGQDs, AKR, and rGQDs/AKR. In the FTIR spectrum of r-GQD, the peaks at 1623 $cm^{-1}$ and 1402 $cm^{-1}$ correspond to the skeleton vibration of the aromatic ring of GQDs, showing the honeycomb lattice of graphene structure.[3, 4] The weak peaks at 2907 $cm^{-1}$ result from the stretching vibration of C-H in the aromatic ring, respectively. In the FTIR spectra of AKR and rGQDs/AKR, we can find the spectral peaks containing N heterocycles obtained from the click reaction of azides and alkynes. The amide I band (1600-1700 $cm^{-1}$) and amide III band (1200-1330 $cm^{-1}$) are often used to analyze the secondary structure of proteins.[5] By comparing the peaks of AKR and rGQDs/AKR in the infrared spectrum of 1250-1750 $cm^{-1}$, it is shown that the assembly with inorganic materials will not change the secondary structure of enzyme protein.[6]

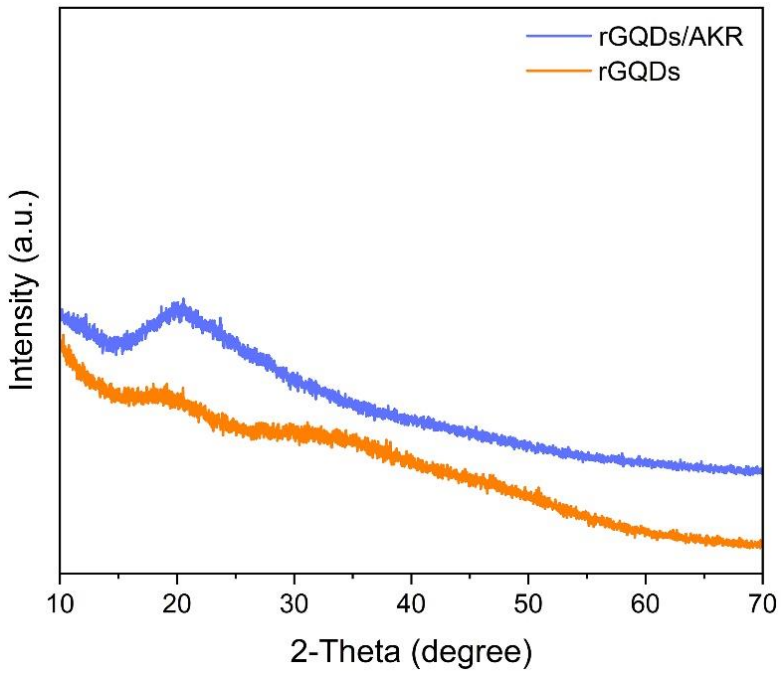


**Figure S9.** XRD patterns of rGQDs, rGQDs/AKR.

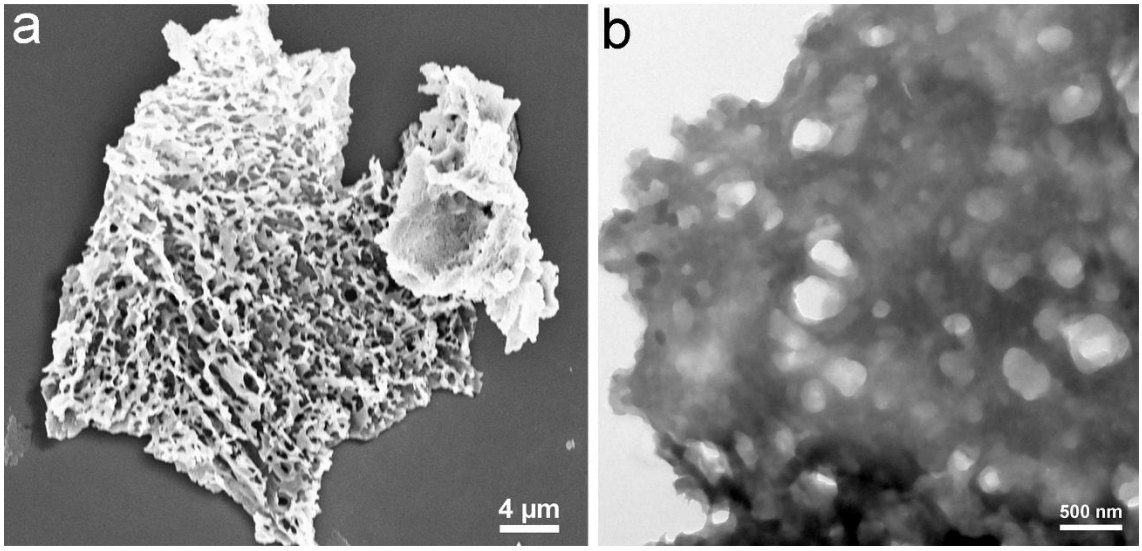


**Figure S10.** (a) SEM and (b) TEM images of rGQDs/AKR.

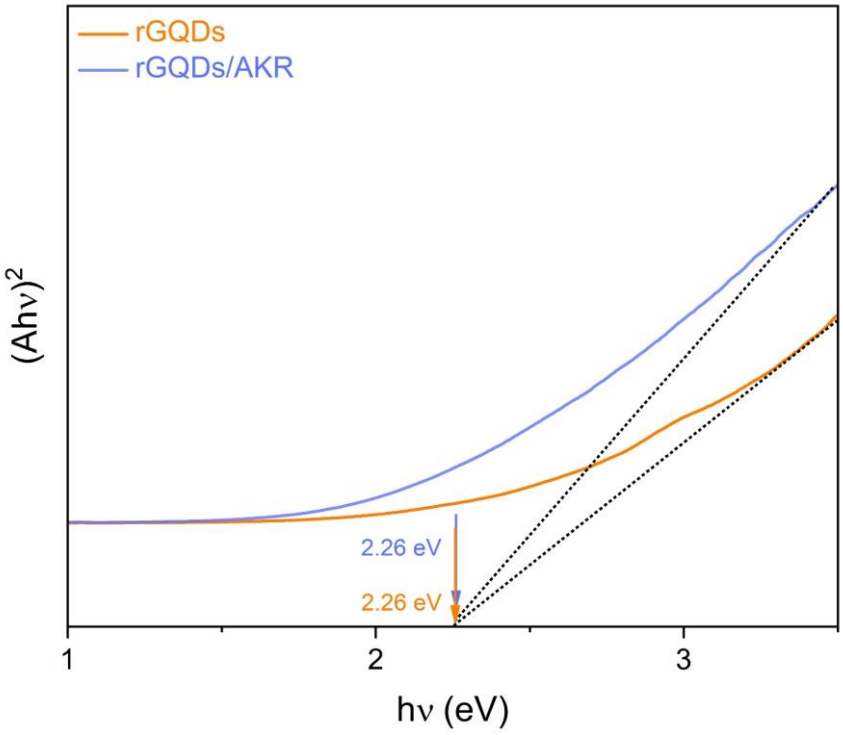


**Figure S11.** The transformed Kubelka-Munk function versus the energy.

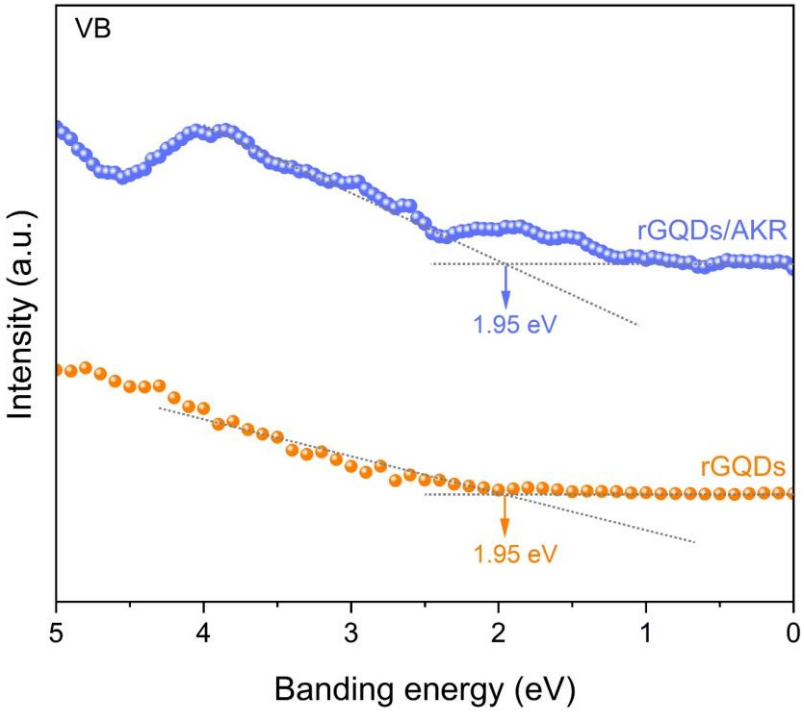


**Figure S12.** XPS spectra: Valence band spectra of rGQDs, rGQDs/AKR.

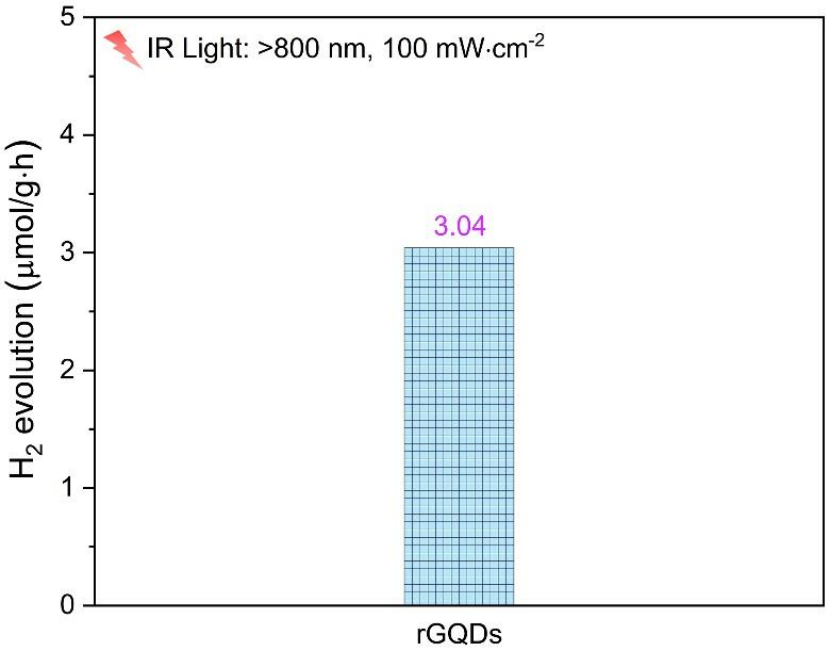


**Figure S13.** Photocatalytic water splitting performance (IR light: > 800 nm, 100 $mW \cdot cm^{-2}$).

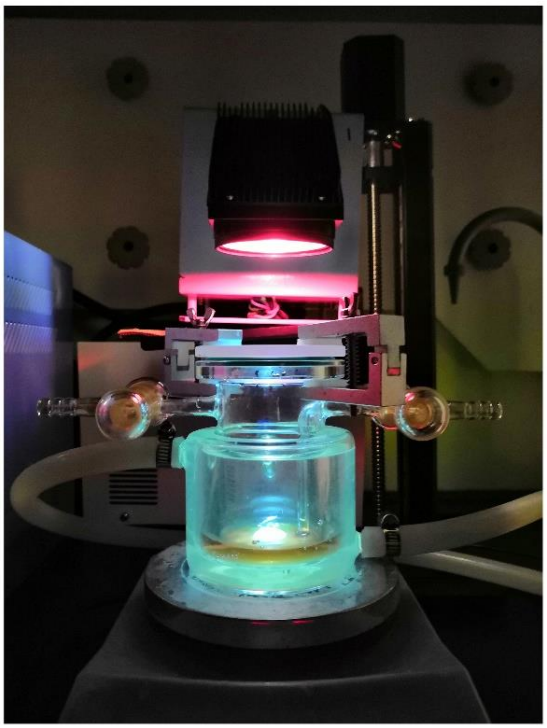

**Figure S14.** The image of an experimental device for photoenzymatic catalysis.

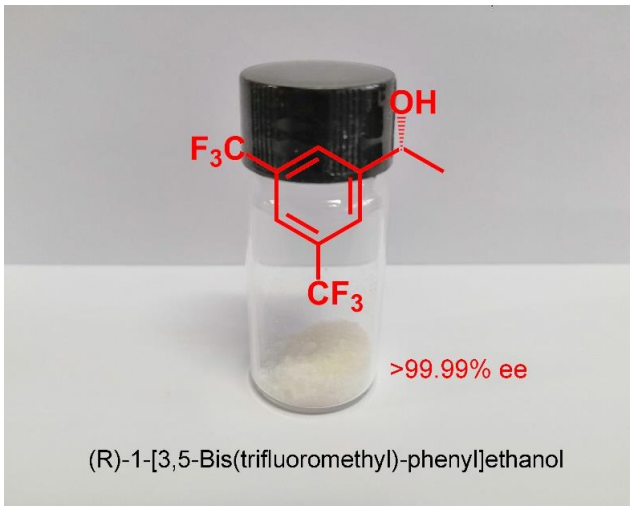


**Figure S15.** The image of photoenzymatic product (R)-3,5-BTPE.

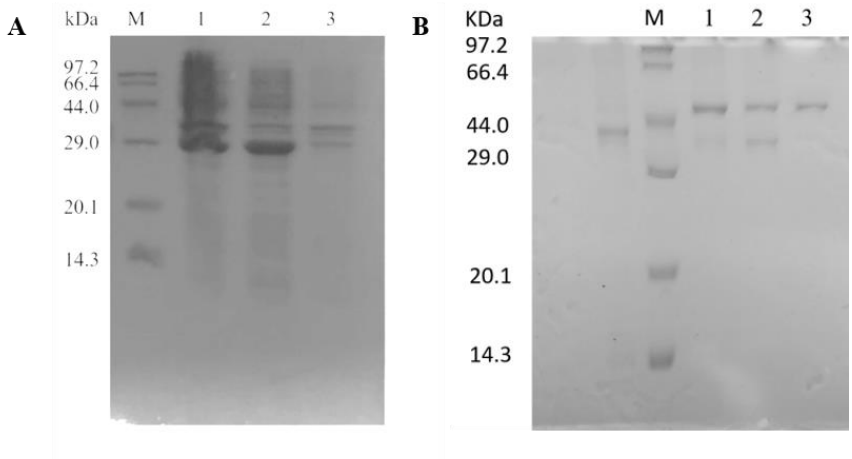


**Figure S16.** SDS PAGEs analysis. (A) lane M: protein marker, lane 1: cell lysate containing imine reductase, lane 2: the cell lysate supernatant, lane 3: the cell lysate precipitate; (B) lane M: protein marker, lane 1: diluted 5 times cell lysate supernatant containing OYE1, lane 2: the undiluted cell lysate supernatant; lane 2: the diluted 30 times cell lysate supernatant.

## 3. Molecular simulations

### 3.1 1. Molecular simulations analysis of rGQDs/AKR

To characterize the effect of rGQD binding on the structure of AKR at the atomic level, molecular dynamics (MD) simulations were conducted with and without NADPH bound to AKR. As determined by TEM and Raman spectroscopy that rGQD has an average size of 2 nm with 2 or 3 layers (**Figure S4** and **S5**), the rGQD model was constructed based on the MD-equilibrated structure of pure carbon dot (CD) cluster,[7] with the starting structure of rGQD consisting of two layers of hexagonal sheet and each edge consisting of six benzene rings. The parameters of rGQD and atomic charges were the same as the report [7] and the AMBER FF99SB force field [8] was used. For AKR, the FF99SB force field was applied as well. And for the cofactor NADPH, parameters reported by Ulf Ryde [9] and GAFF force field [10] were applied. Considering the molecular size and property of rGQD, molecular docking can hardly give accurate prediction of binding site on AKR. Therefore, to investigate the effect of initial relative position between rGQD and AKR on the binding, four cases of rGQDs–AKR with each under a distance of 30 Å between rGQD and AKR surfaces were subjected directly to MD simulations, with or without NADPH bound (**Figure S14 and S15**). Such strategy would increase the sampling of binding patterns and reduce the impact of artifacts caused by selection of binding modes from molecular docking calculations.

MD simulations were performed by using the Amber22 software.[11] Each complex (solute) was immersed into the center of a truncated octahedron box of TIP3P water molecules with a margin distance of 10.0 Å, $Na^+$ counterions were added to keep system

in electroneutrality. The system was firstly energy minimized by the steepest descent method for 5000 steps with the solute restricted by a harmonic constraint of 100 kcal·mol$^{-1}$Å$^{-2}$, followed by a conjugate gradient minimization of 5000 steps with no constraint. Then the system was gradually heated from 0 K to 300 K under the NVT ensemble over a period of 1 ns, during which the Langevin thermostat with a coupling coefficient of 1.0 ps and a weak constraint of 10 kcal·mol$^{-1}$Å$^{-2}$ on the solute was applied. The system was further subjected to an equilibrium simulation for 5 ns by removing all constraints. Finally, a production MD simulation with a time scale of 400 ns was conducted under the NPT ensemble. Periodic boundary conditions were applied. System temperature was kept constant at 300 K by using the Berendsen thermostat with a time constant of 1 ps. Isotropic constant pressure was maintained by using the Berendsen pressure coupling algorithm with a time constant of 1 ps. Hydrogens that involve in covalent bonds were constrained by using the SHAKE algorithm.[12] The long-range electrostatic interactions were treated by the Particle Mesh Ewald (PME) method.[13] The cutoffs for both long-range electrostatic and van der Waals (vdW) interactions were set to 10.0 Å. The time step was set to 2 fs and the coordinates were saved every 10 ps to record the MD trajectory.

### 3.2 Enantioselective mechanism of rGQD/AKR towards 3,5-BTAP.

To explore the enantioselective catalytic mechanism of rGQD/AKR towards 3,5-BTAP, molecular docking and MD simulations were performed. The structure of 3,5-BTAP was constructed with the GaussView software (version 6.0.16) [14] and was optimized with the density functional theory (DFT) at the level of B3LYP/6-31G(d) by using the Gaussian 16 software (version C.01).[15] The optimized 3,5-BTAP served as ligand in molecular docking. To investigate the effect of NADPH on the enantioselectivity of AKR, the crystal structures of AKR–$NADP^+$–Epalrestat (PDB ID: 6KIY) [16] and AKR–Tolrestat (PDB ID: 6KIK) [16] were retrieved from the RCSB Protein Data Bank and were used as receptors by removing crystal waters and the co-crystalized inhibitors (Epalrestat and Tolrestat) and converting $NADP^+$ to NADPH with the UCSF ChimeraX software (version 1.8).[17] As binding of rGQD would not hinder the binding of substrate or change the conformation of AKR catalytic domain, simplified models were used without rGQD included. The AutoDock Vina software (version 1.2.5) [18] was applied for docking calculations. A cubic box of 60×60×60 girds with the grid spacing of 0.375 Å and the box center superimposed with the geometric center of the original binding inhibitors was used to define the docking space. Six rounds of docking calculations for each of AKR–NADPH and AKR were performed, with the exhaustiveness ranging from 15 to 25 at an interval of 2. The docked 3,5-BTAP that showed the most negative binding energies and the highest repeatability were regarded as the bioactive binding conformations.

The structures of AKR–NADPH–3,5-BTAP and AKR–3,5-BTAP derived from

molecular docking were subjected to MD simulations. The FF19SB force field and the Ulf Ryde reported parameters together with the GAFF force field were applied for AKR cofactor NADPH, respectively. And for the substrate 3,5-BTAP, GAFF force field parameters together with the restricted electrostatic potential (RESP) atomic charges [19] which were generated based on the optimized structure by following the reported procedure were used.[20] The MD simulation procedures were the same as described above.

AoIRED showed a compromised enantioselectivity towards the substrate 1-methyl-3,4-dihydroisoquinoline as indicated by our experimental data (**Figure S24c**). The binding features of AoIRED and 1-methyl-3,4-dihydroisoquinoline were explored through molecular simulations for comparison, with and without NADPH included. The crystal structures of 5FWN [21] and 5A9S [21] were used for constructing the binding complexes of AoIRED–NADPH–1-methyl-3,4-dihydroisoquinoline and AoIRED–1-methyl-3,4-dihydroisoquinoline, respectively. The docking space was defined according to the location of crystalized catalytic product (1R)-1-methyl-1,2,3,4-tetrahydroisoquinoline in 5FWN. The procedures of molecular docking and MD calculations together with the parameters and force fields used were the same as above.

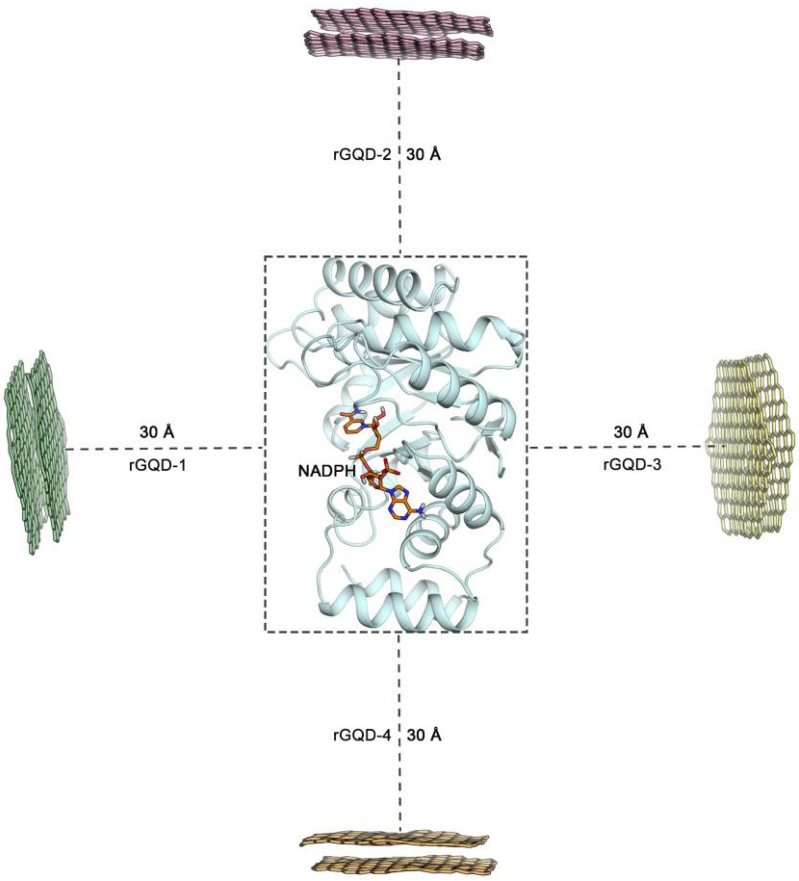


**Figure S17.** Initial structures of rGQD–AKR–NADPH for molecular dynamics (MD) simulation. rGQD was respectively positioned at four directions with a distance of 30 Å relative to the surface of AKR (denoted as rGQD-1, rGQD-2, rGQD-3, and rGQD-4), each combination was subjected to MD simulation independently.

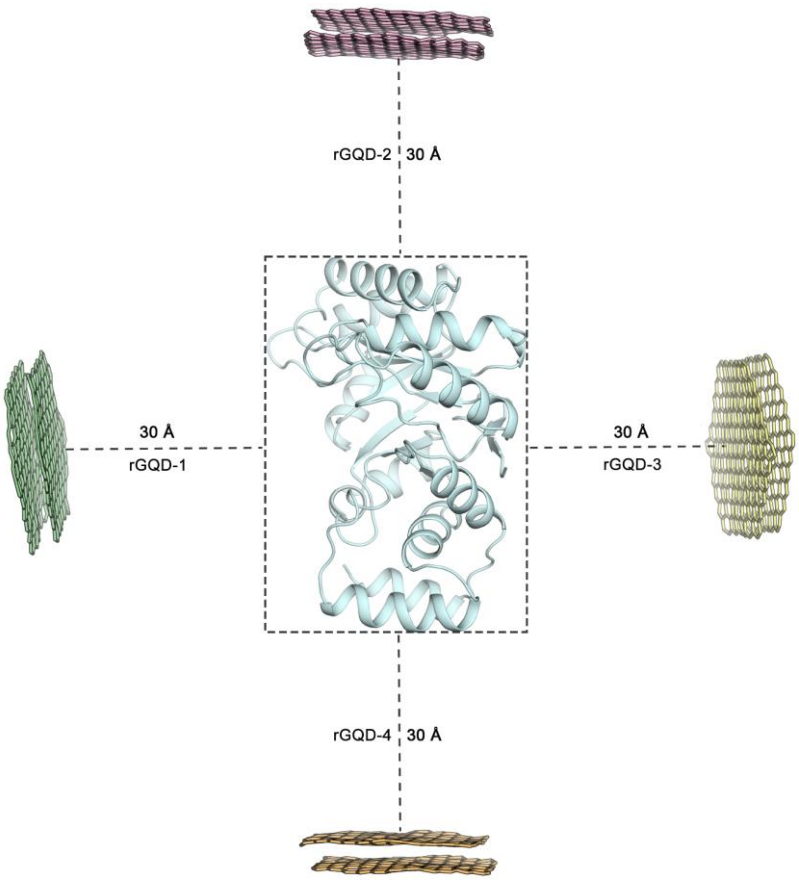


**Figure S18.** Initial structures of rGQD–AKR for molecular dynamics (MD) simulation. rGQD was respectively positioned at four directions with a distance of 30 Å relative to the surface of AKR (denoted as rGQD-1, rGQD-2, rGQD-3, and rGQD-4), each combination was subjected to MD simulation independently.

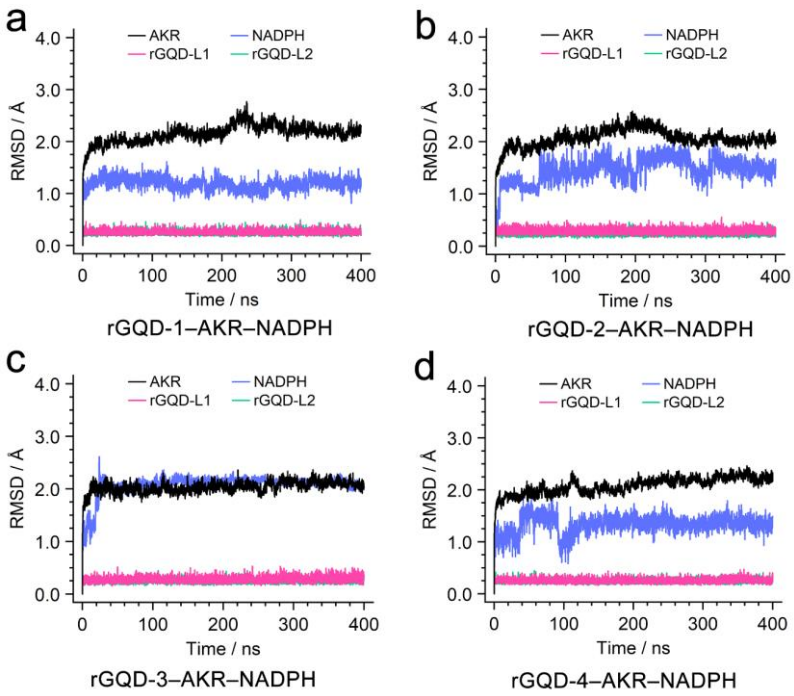


**Figure S19.** Root mean squared deviation (RMSD) profiles of the rGQD–AKR–NADPH binding complexes across MD simulations. a–d, RMSD profiles of AKR, NADPH, and the rGQD layers of rGQD-1, rGQD-2, rGQD-3, and rGQD-4, resplectively. The two layers of rGQD were denoted as rGQD-L1 and rGQD-L2, respectively.

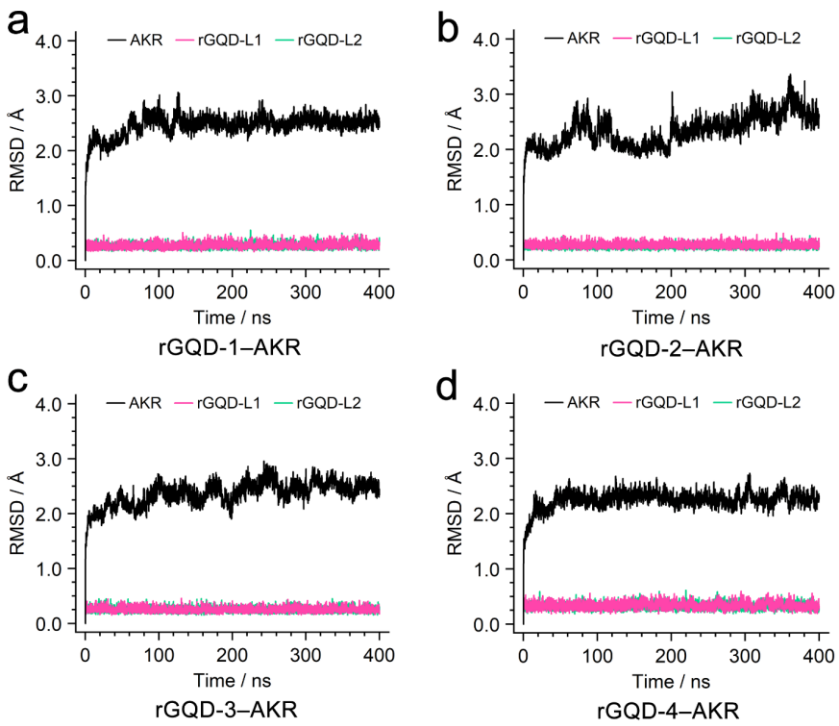


**Figure 20.** Root mean squared deviation (RMSD) profiles of the rGQD–AKR binding complexes across MD simulations. a–d, RMSD profiles of AKR and the rGQD layers of rGQD-1, rGQD-2, rGQD-3, and rGQD-4, resplectively. The two layers of rGQD were denoted as rGQD-L1 and rGQD-L2, respectively.

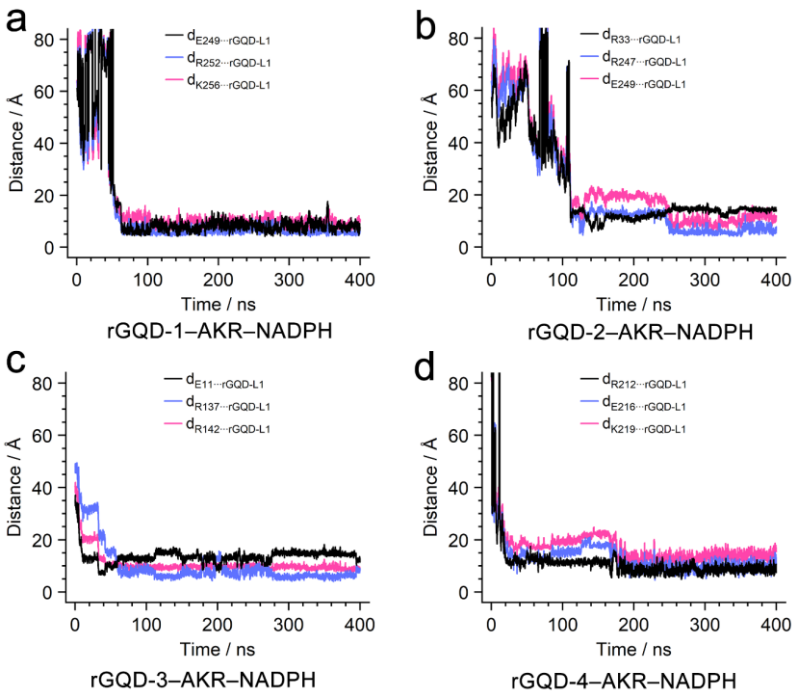


**Figure S21.** Profiles of key distances in the rGQD–AKR–NADPH binding complexes. AKR residues with the sidechain groups forming cation−π or anion−π interactions were identified as key residues to the binding of rGQD. a–d, the presented distances were calculated between the geometric centers of the cation/anion AKR sidechain groups and the geometric centers of first layers of rGQD1, rGQD2, rGQD3, and rGQD4 (denoted as rGQD-L1).

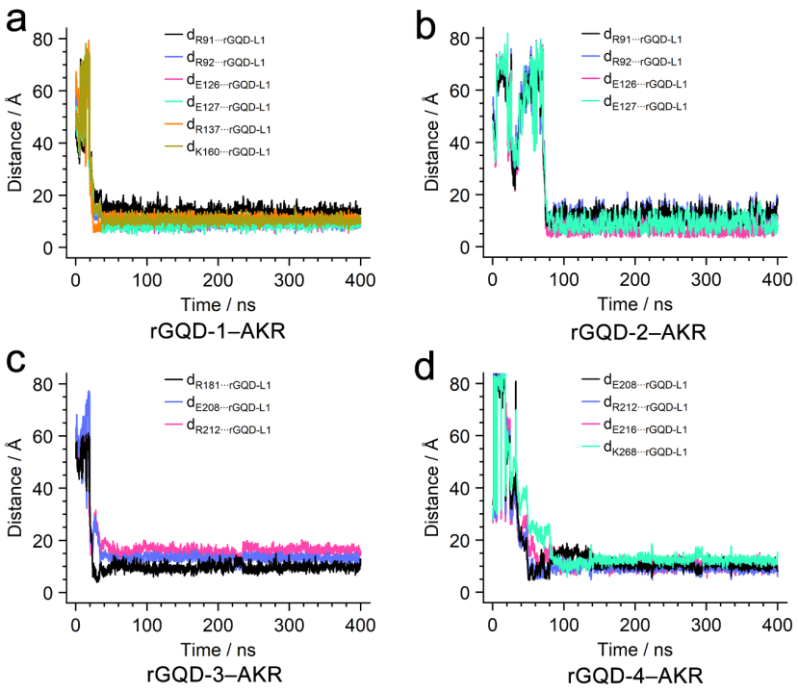


**Figure S22.** Profiles of key distances in the rGQD–AKR binding complexes. AKR residues with the sidechain groups forming cation−π or anion−π interactions were identified as key residues to the binding of rGQD. a–d, the presented distances were calculated between the geometric centers of the cation/anion AKR sidechain groups and the geometric centers of first layers of rGQD1, rGQD2, rGQD3, and rGQD4 (denoted as rGQD-L1).

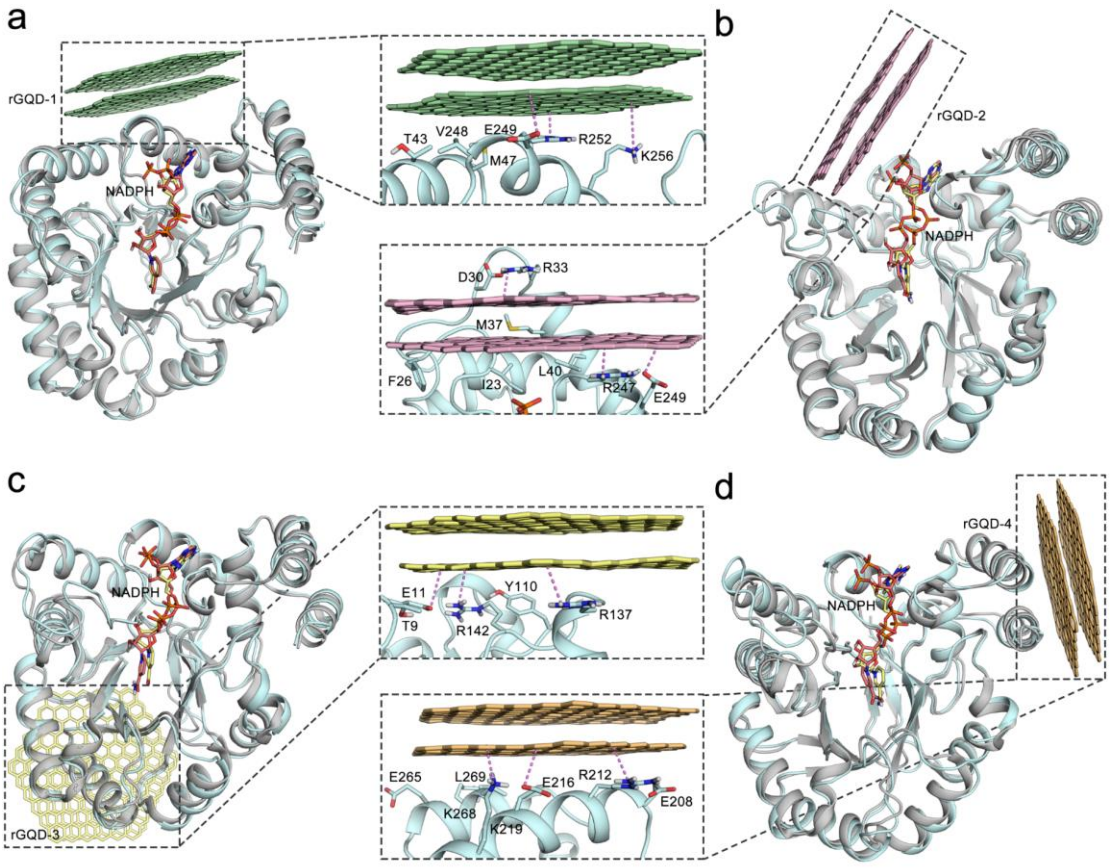


**Figure S23.** Superimposition of the equilibrated binding conformations of rGQD–AKR-NADPH (AKR in cyan cartoon, NADPH in dark salmon stick) and the crystal structure of AKR-NADPH (PDB ID: 6KIY. AKR in grey cartoon, NADPH in light yellow stick). a–d, the equilibrated overall binding complexes of rGQD-1/rGQD-2/rGQD-3/rGQD-4–AKR-NADPH respectively, with the intermolecular interactions shown in the enlarged illustrations. The cation−π and anion−π interactions between rGQD and the surrounding residues were indicated by pink dotted lines.

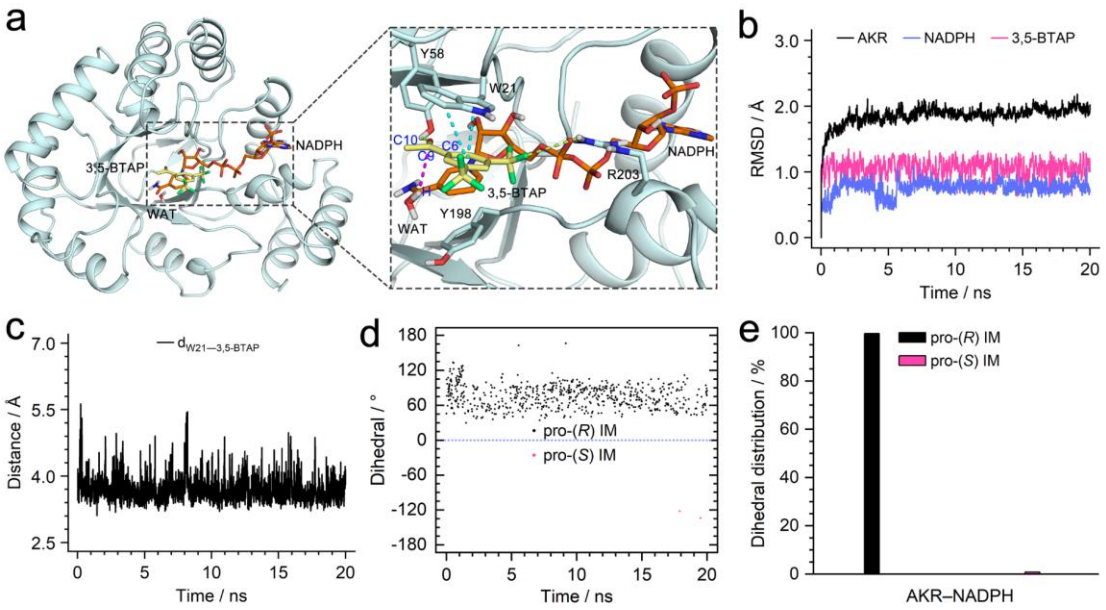


**Figure S24.** MD simulation of the AKR-NADPH – 3,5-BTAP binding complex. a, equilibrated binding conformation of AKR-NADPH – 3,5-BTAP. b, RMSD profiles of the binding components. c, profile of the distance between the geometric centers of W21 sidechain and aromatic ring of 3,5-BTAP. d and e, value and distribution of the key improper dihedral ∠C6-C10-C9-H across the MD simulation.

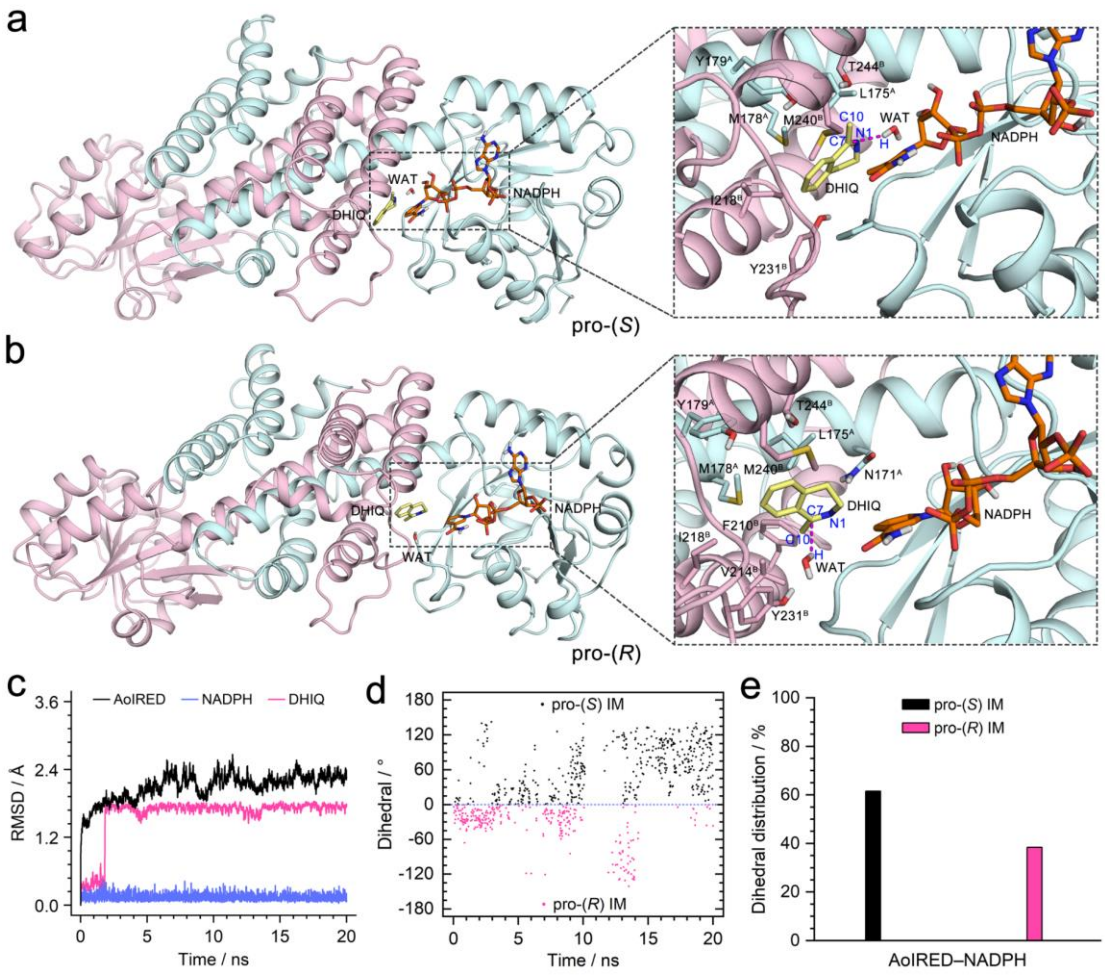


**Figure S25.** MD simulation of the AoIRED-NADPH–DHIQ binding complex. a, the representative pro-(*S*) binding form of AoIRED-NADPH–DHIQ based on cluster analysis of MD trajectory. b, the representative pro-(*R*) binding form of AoIRED-NADPH–DHIQ based on cluster analysis of MD trajectory. c, RMSD profiles of the binding components. d and e, value and distribution of the key improper dihedral ∠N1-C10-C7-H across the MD simulation.

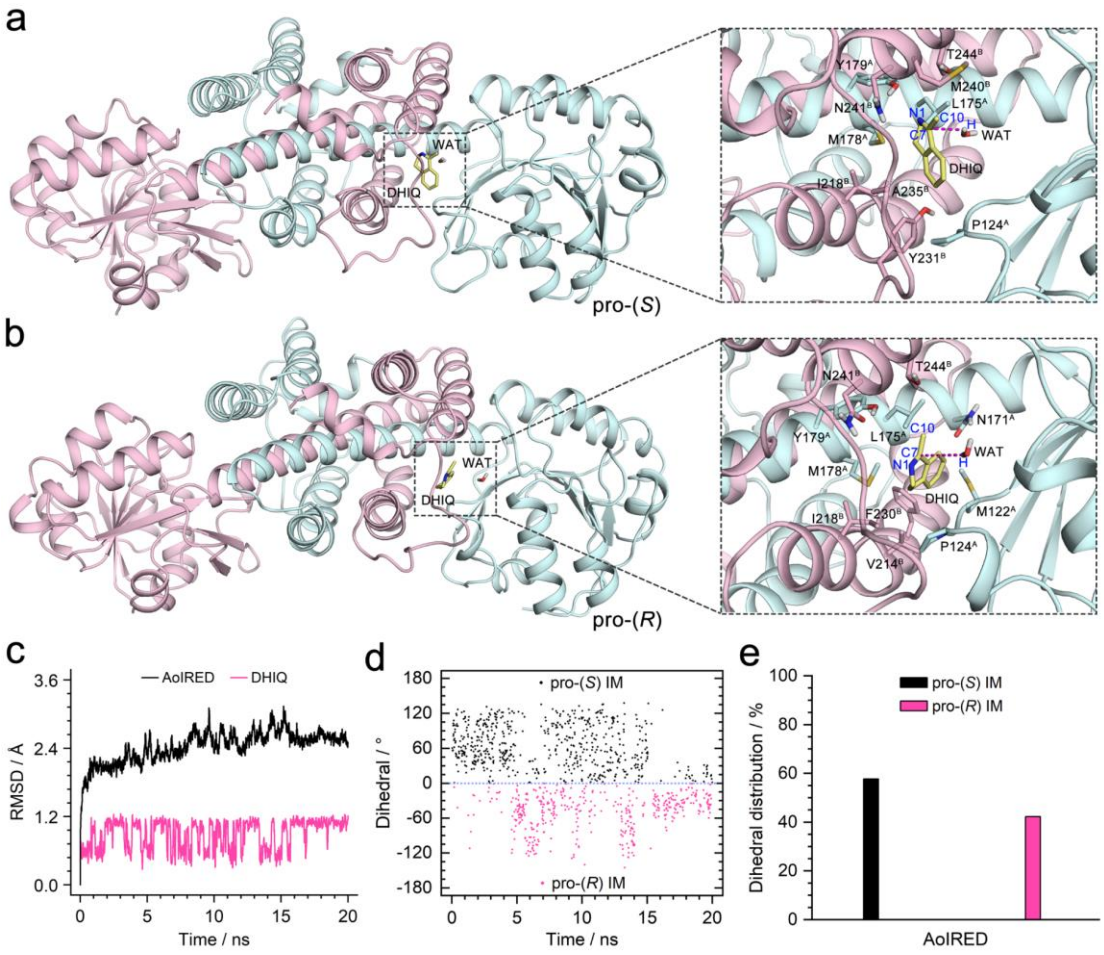


**Figure S26.** MD simulation of the AoIRED–DHIQ binding complex. a, the representative pro-(*S*) binding form of AoIRED–DHIQ based on cluster analysis of MD trajectory. b, the representative pro-(*R*) binding form of AoIRED–DHIQ based on cluster analysis of MD trajectory. c, RMSD profiles of the binding components. c, RMSD profiles of the binding components. d and e, value and distribution of the key improper dihedral ∠N1-C10-C7-H across the MD simulation.

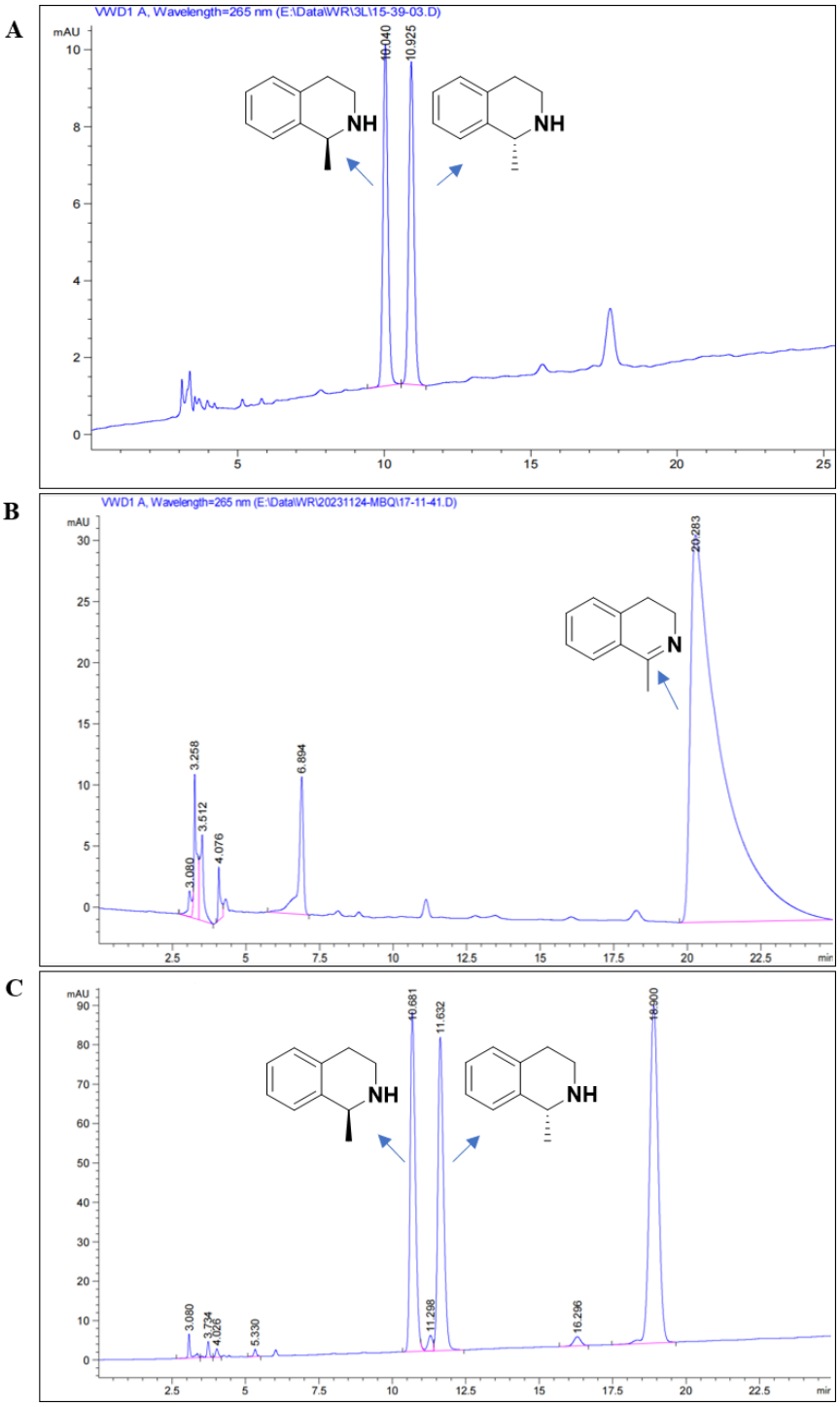


**Figure S27.** Normal-phase HPLC analysis of reference standard: 1-methyl-1,2,3,4-tetrahydroisoquinolin raceme (A) and 1-methyl-3,4-dihydroisoquinolin (B); and normal-phase HPLC analysis of 1-methyl-1,2,3,4-tetrahydroisoquinolin (C) using IR-driven AoIRED-rGQD catalysis.

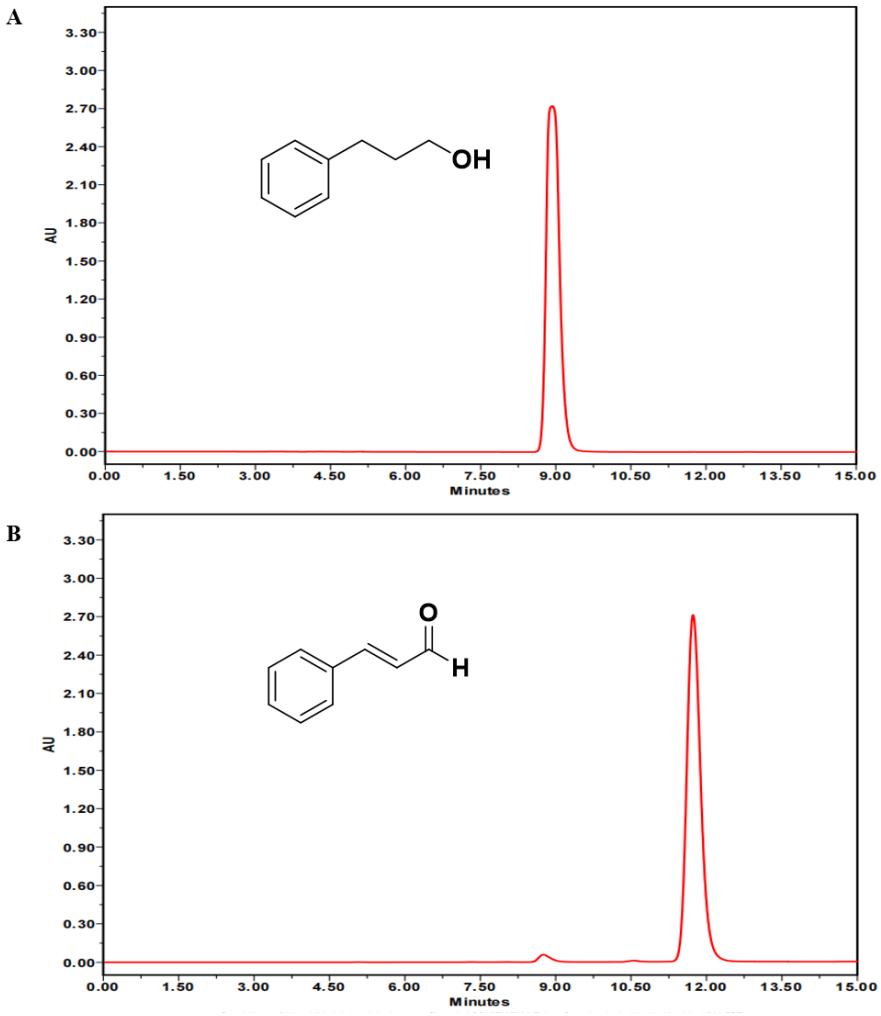


**Figure S28.** Reversed phase HPLC analysis of reference standard: cinnamaldehyde (A) and 3-phenylpropanol (B).

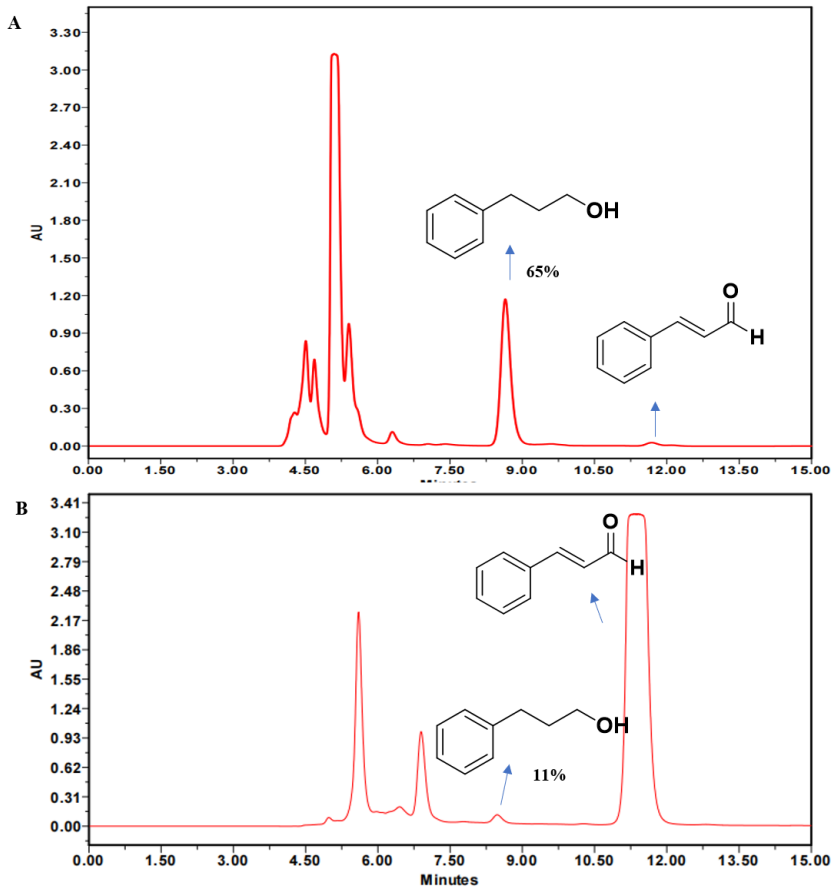


**Figure S29.** Reversed phase HPLC analysis of IR-driven OYE1-rGQD catalyzed reduction of cinnamaldehyde in the absence of electron mediator and oxidation state cofactor (A) or the presence of electron mediator and oxidation state cofactor (B).

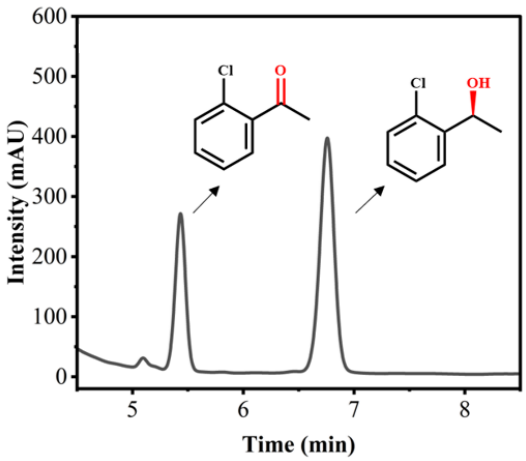


**Figure S30.** HPLC analysis result of isotopic tracer experimental reaction. The corresponding product *S*-configured 1-(2-chlorophenyl)ethan-1-*d*-1-ol-*d* obtained a 54% yield.

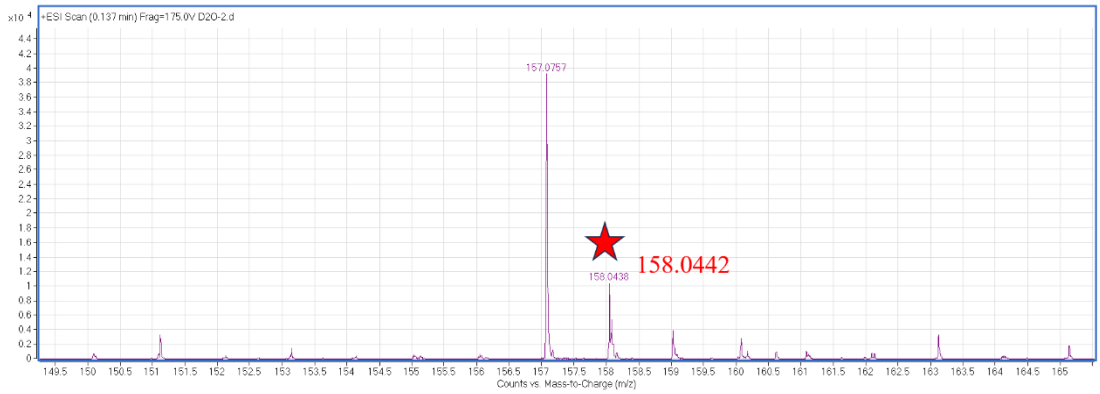


**Figure S31.** HRMS analysis of isotopic tracer experimental reaction. (HRMS (ESI) m/z [M] Calcd. for $C_8H_7D_2ClO$: 158.0467; found: 158.0442).

## Reference


1. Chin, J. W.; Santoro, S. W.; Martin, A. B.; King, D. S.; Wang, L.; Schultz, P. G., Addition of p-azido-L-phenylalanine to the genetic code of Escherichia coli. *Journal of the American Chemical Society* **2002,** *124* (31), 9026-7.
2. Novoselov, K. S.; Jiang, D.; Schedin, F.; Booth, T.; Khotkevich, V.; Morozov, S.; Geim, A. K., Two-dimensional atomic crystals. *Proceedings of the National Academy of Sciences* **2005,** *102* (30), 10451-10453.
3. Chen, W.; Li, D.; Tian, L.; Xiang, W.; Wang, T.; Hu, W.; Hu, Y.; Chen, S.; Chen, J.; Dai, Z., Synthesis of graphene quantum dots from natural polymer starch for cell imaging. *Green Chemistry* **2018,** *20* (19), 4438-4442.
4. Ali, S.; Sikdar, S.; Basak, S.; Roy, D.; Dakua, V. K.; Adhikary, P.; Roy, M. N., High Visual Colorimetric Determination of F- Ions by Exploiting the Inhibition of Oxidase Mimicking Activity of FeMnO4@GQD Nanocomposite. *ChemistrySelect* **2022,** *7* (30), e202201186.
5. Yang, H.; Yang, S.; Kong, J.; Dong, A.; Yu, S., Obtaining information about protein secondary structures in aqueous solution using Fourier transform IR spectroscopy. *Nature protocols* **2015,** *10* (3), 382-396.
6. Li, X.; Bai, Y.; Huang, Z.; Si, C.; Dong, Z.; Luo, Q.; Liu, J., A highly controllable protein self-assembly system with morphological versatility induced by reengineered host–guest interactions. *Nanoscale* **2017,** *9* (23), 7991-7997.
7. Paloncýová, M.; Langer, M.; Otyepka, M., Structural Dynamics of Carbon Dots in Water and N,N-Dimethylformamide Probed by All-Atom Molecular Dynamics Simulations. *Journal of Chemical Theory and Computation* **2018,** *14* (4), 2076-2083.
8. Hornak, V.; Abel, R.; Okur, A.; Strockbine, B.; Roitberg, A.; Simmerling, C., Comparison of multiple Amber force fields and development of improved protein backbone parameters. *Proteins: Structure, Function, and Bioinformatics* **2006,** *65* (3), 712-725.
9. Holmberg, N.; Ryde, U.; Bülow, L., Redesign of the coenzyme specificity in l-Lactate dehydrogenase from Bacillus stearothermophilus using site-directed mutagenesis and media engineering. *Protein Engineering, Design and Selection* **1999,** *12* (10), 851-856.
10. Wang, J.; Wolf, R. M.; Caldwell, J. W.; Kollman, P. A.; Case, D. A., Development and testing of a general amber force field. *Journal of Computational Chemistry* **2004,** *25* (9), 1157-1174.
11. Case, D. A.; Cheatham Iii, T. E.; Darden, T.; Gohlke, H.; Luo, R.; Merz Jr, K. M.; Onufriev, A.; Simmerling, C.; Wang, B.; Woods, R. J., The Amber biomolecular simulation programs. *Journal of Computational Chemistry* **2005,** *26* (16), 1668-1688.
12. Ryckaert, J.-P.; Ciccotti, G.; Berendsen, H. J. C., Numerical integration of the cartesian equations of motion of a system with constraints: molecular dynamics of n-alkanes. *Journal of Computational Physics* **1977,** *23* (3), 327-341.
13. Essmann, U.; Perera, L.; Berkowitz, M. L.; Darden, T.; Lee, H.; Pedersen, L. G., A smooth particle mesh Ewald method. *The Journal of Chemical Physics* **1995,**

*103* (19), 8577-8593.
14. Crespi, S.; Fagnoni, M., Generation of Alkyl Radicals: From the Tyranny of Tin to the Photon Democracy. *Chem Rev* **2020,** *120* (17), 9790-9833.
15. Prier, C. K.; Rankic, D. A.; MacMillan, D. W., Visible light photoredox catalysis with transition metal complexes: applications in organic synthesis. *Chem Rev* **2013,** *113* (7), 5322-63.
16. Zhang, C.; Min, Z.; Liu, X.; Wang, C.; Wang, Z.; Shen, J.; Tang, W.; Zhang, X.; Liu, D.; Xu, X., Tolrestat acts atypically as a competitive inhibitor of the thermostable aldo-keto reductase Tm1743 from Thermotoga maritima. *FEBS Letters* **2020,** *594* (3), 564-580.
17. Meng, E. C.; Goddard, T. D.; Pettersen, E. F.; Couch, G. S.; Pearson, Z. J.; Morris, J. H.; Ferrin, T. E., UCSF ChimeraX: Tools for structure building and analysis. *Protein Science* **2023,** *32* (11), e4792.
18. Trott, O.; Olson, A. J., AutoDock Vina: Improving the speed and accuracy of docking with a new scoring function, efficient optimization, and multithreading. *Journal of Computational Chemistry* **2010,** *31* (2), 455-461.
19. Bayly, C. I.; Cieplak, P.; Cornell, W.; Kollman, P. A., A well-behaved electrostatic potential based method using charge restraints for deriving atomic charges: the RESP model. *The Journal of Physical Chemistry* **1993,** *97* (40), 10269-10280.
20. Dupradeau, F.-Y.; Pigache, A.; Zaffran, T.; Savineau, C.; Lelong, R.; Grivel, N.; Lelong, D.; Rosanski, W.; Cieplak, P., The R.E.D. tools: advances in RESP and ESP charge derivation and force field library building. *Physical Chemistry Chemical Physics* **2010,** *12* (28), 7821-7839.
21. Aleku, G. A.; Man, H.; France, S. P.; Leipold, F.; Hussain, S.; Toca-Gonzalez, L.; Marchington, R.; Hart, S.; Turkenburg, J. P.; Grogan, G.; Turner, N. J., Stereoselectivity and Structural Characterization of an Imine Reductase (IRED) from Amycolatopsis orientalis. *ACS Catalysis* **2016,** *6* (6), 3880-3889.